

NEW ALGEBRAIC FAST ALGORITHMS FOR N -BODY PROBLEMS IN TWO AND THREE DIMENSIONS

RITEESH KHAN* AND SIVARAM AMBIKASARAN†

Abstract. This article presents two new algebraic algorithms to perform fast matrix-vector product for N -body problems in d dimensions, namely $nHODLRdD$ (nested algorithm) and $s-nHODLRdD$ (semi-nested or partially nested algorithm). The $nHODLRdD$ and $s-nHODLRdD$ algorithms are the nested and semi-nested version of our previously proposed fast algorithm, the hierarchically off-diagonal low-rank matrix in d dimensions ($HODLRdD$) [25], respectively, where the admissible clusters are the certain far-field and the vertex-sharing clusters. We rely on algebraic low-rank approximation techniques (ACA and NCA) and develop both algorithms in a black-box (kernel-independent) fashion. The initialization time of the proposed hierarchical structures scales quasi-linearly. Using the $nHODLRdD$ and $s-nHODLRdD$ hierarchical structures, one can perform the multiplication of a dense matrix (arising out of N -body problems) with a vector that scales as $\mathcal{O}(pN)$ and $\mathcal{O}(pN \log(N))$, respectively, where p grows at most poly logarithmically¹ with N . Another noteworthy contribution of this article is that we perform a comparative study of the two proposed algorithms with five different algebraic fast matrix-vector product algorithms (fast algorithms with nested and non-nested bases like two different algebraic variants of the Fast Multipole Method, $HODLRdD$, \mathcal{H} matrix algorithms) for two and three dimensions problems. All the algorithms are tested on various kernel functions in 2D and 3D with different distributions of particles. We apply these fast matrix-vector algorithms to get fast iterative solution of a dense system arising out of the discretized integral equations and radial basis functions interpolation. Also, the article discusses the performance comparison, scalability and provides various benchmarks. All the algorithms are implemented in the same fashion using C++ and tested within the same environment, allowing for meaningful comparisons. To the best of our knowledge, this is the first work to study the performance analysis of different algebraic fast matrix-vector product algorithms for 2D and 3D problems. The numerical results in 2D and 3D ($d = 2, 3$) show that the proposed $nHODLRdD$ algorithm is competitive to the algebraic Fast Multipole Method in d dimensions with respect to the matrix-vector product time and space complexity. The C++ implementation with OpenMP parallelization of the proposed algorithms is available at <https://github.com/riteshkhan/nHODLRdD/>.

Key words. N -body problems, Hierarchical matrices, Weak admissibility, \mathcal{H}^2 matrices, ACA, Nested cross approximation

AMS subject classifications. 65F55, 65D12, 65R20, 65D05, 65R10

1. Introduction. N -body problems are frequently encountered in many applications such as solving PDEs [18], integral equations [23], radial basis function (RBF) interpolation [11], electromagnetic scattering [10], Gaussian process regression [29], machine learning [17], kernel density estimation [34], inverse problems [31], etc. Matrices arising from the N -body problems are usually large and dense. A direct evaluation of the product of such $N \times N$ matrix with vector is prohibitive as its time and space complexity scale as $\mathcal{O}(N^2)$. However, these matrices possess rank-structuredness, which can be leveraged to store and perform matrix operations. The literature on the rank-structuredness of matrices is vast, and we refer the reader to a few selected developments on this front [36, 4, 18, 14, 1, 2, 24, 27, 12, 22, 26, 9, 33].

In the past decades, various algorithms have been developed to perform the matrix-vector product efficiently. One of the first works in this area was the Barnes-Hut algorithm [4] or Tree code, which reduces the matrix-vector product complexity from $\mathcal{O}(N^2)$ to $\mathcal{O}(N \log(N))$. Greengard and Rokhlin propose the Fast Multipole Method (from now on abbreviated as FMM) [18, 19], which further reduces the matrix-vector product cost to $\mathcal{O}(N)$. After that, various FMM-like kernel-independent algorithms [35] were proposed, primarily based on analytic expansions. Hackbusch and collaborators [9, 8] are the pioneers to interpret certain sub-blocks (sub-matrices) of the matrices arising from N -body problems as low-rank and provide an important theoretical framework. In [9, 8, 16], they discuss the standard (or strong) admissibility criterion, i.e., where the separation distance between two clusters exceeds the diameter of either cluster. It is to be noted that the FMM (\mathcal{H}^2 with standard admissibility) and the Tree code (\mathcal{H} with standard admissibility) are based on the standard or strong admissibility criterion. In their subsequent work [22], they study the rank of kernel matrices arising out of 1D distribution of particles. This article shows the rank of interaction between the neighboring clusters in 1D, i.e., the clusters satisfying the *weak admissibility condition* scale $\mathcal{O}(\log(N))$. This work doesn't discuss the rank of the interaction of neighboring clusters in higher dimensions ($d > 1$) (though they state that higher dimensions will be considered later and refer to an article in the bibliography. However, to the best of our knowledge and searches, the article was never published or is available to the

*Department of Mathematics, IIT Madras, Chennai, India. khanritesh28@gmail.com

†Department of Mathematics and Robert Bosch Centre for Data Science & Artificial Intelligence, IIT Madras, Chennai, India. sivaambi@alumni.stanford.edu

¹ $p \in \mathcal{O}(\log^\alpha(N))$. To be precise, the proposed algorithms scale at most quasi-linearly, i.e., $\mathcal{O}(N \log^\alpha(N))$, $\alpha \geq 0$

public). It is to be noted that the extension of this idea, i.e., compressing all the non-self interactions, will not result in a quasi-linear matrix-vector product algorithm in higher dimensions because the rank of the nearby clusters grows in d dimensions as $\mathcal{O}(N^{(d-1)/d} \log(N))$ [23, 24, 25]. Further, it is to be noted that some of the hierarchical matrices such as HODLR [2], HSS [33, 12], HBS [15], \mathcal{H} -matrices with weak admissibility [22], MHS [32], BLR [3], etc rely on representing certain or all nearby interactions as low-rank matrices.

In our recent work [25], we have shown that the rank of the far-field and vertex-sharing clusters do not scale with any positive power of N . Hence, admissibility of the far-field and vertex-sharing clusters *could be* a way to extend the notion of *weak admissibility condition* in higher dimensions. Based on this proposed *weak admissibility condition*, we developed a matrix-vector product algorithm in d dimensions with quasi-linear complexity, namely the hierarchically off-diagonal low-rank matrix in d dimensions (from now on abbreviated as *HODLRdD*). *Our main focus in this article is to develop nested versions of the HODLRdD algorithm in a purely algebraic way, which performs better than the HODLRdD algorithm.*

In this article, we present two new algorithms for fast matrix-vector product in d dimensions, which are faster than the previously proposed *HODLRdD* algorithm [24, 25]. The first algorithm we propose is the nested hierarchically off-diagonal low-rank matrix in d dimensions (from now on abbreviated as *nHODLRdD*), which scales as $\mathcal{O}(pN)$. The *nHODLRdD* algorithm is the nested ¹ version of the *HODLRdD* algorithm [25] and a special subclass of the \mathcal{H}^2 matrix. Due to the use of nested bases, the time and space complexities are reduced compared to the *HODLRdD* algorithm. The numerical experiments in 2D and 3D ($d = 2, 3$) show that the *nHODLRdD* algorithm is competitive to the algebraic FMM in d dimensions with respect to the matrix-vector product time and space complexity. The second algorithm we develop in this article is the semi-nested ² version of the *HODLRdD* algorithm (from now on abbreviated as *s-nHODLRdD*), whose matrix-vector product time complexity scales as $\mathcal{O}(pN \log(N))$. The *s-nHODLRdD* algorithm can be thought of as a cross of \mathcal{H}^2 and \mathcal{H} matrices. The constants in front of the complexity estimates depend on the given tolerance. We develop all the algorithms in this article using algebraic techniques, which makes the algorithms kernel-independent, i.e., only access to the matrix entries is enough. Therefore, all the **seven** fast algorithms (Table 7) in this article are black-box algorithms.

2. Related works and novelty of our work. The matrices arising out of N -body problems possess rank-structuredness, i.e., certain sub-blocks of these matrices can be approximated by a low-rank representation. The construction of the low-rank approximation has been studied extensively. One can categorize the low-rank approximation techniques into two classes (i) Algebraic techniques (SVD, RRQR [13], RRLU [28], ACA [5], etc.) and (ii) Analytic techniques (Analytic series expansions [18, 19], Interpolation [14], etc.). Both the algebraic and analytic techniques have their advantages and disadvantages. In this article, we choose algebraic techniques for the following reasons.

1. Algebraic techniques only require access to the matrix entries and can be used in a black-box fashion; they neither need any series expansions of the underlying kernel function nor the knowledge of the kernel function.
2. The rank of the compressed clusters obtained using algebraic techniques is usually lower than that obtained from analytic techniques, as algebraic techniques are domain and problem-specific.
3. Algebraic techniques are more efficient than analytical techniques when dealing with data sets of higher dimensions.
4. The article focuses on developing an efficient nested version of a hierarchical structure based on the *weak admissibility* condition [25]. Algebraic techniques are helpful in this case.

We refer the readers to [36] and the references therein for a detailed discussion of various techniques and benchmarks. Since the main focus of this article is to develop efficient nested and semi-nested fast algorithms using algebraic techniques, in this section, we discuss some existing works that study different algebraic techniques and those in line with this article. The \mathcal{H} matrix [22, 21] is one of the most commonly used frameworks to handle the large dense matrices arising from the N -body problems. Though the \mathcal{H} matrix algorithm is fast, it can be further accelerated using the nested form of the bases, which leads to \mathcal{H}^2 matrix algorithm [7, 8]. It has been demonstrated that the \mathcal{H}^2 matrix is a more efficient framework than the \mathcal{H} matrix regarding time and storage. Several kernel-independent algorithms have been developed to efficiently construct the \mathcal{H}^2 matrix. Börm [7] proposes an $\mathcal{O}(N \log(N))$ algorithm to construct \mathcal{H}^2 matrix in a purely

¹Nested bases are used for the **entire** interaction list of a cluster

²We call it semi-nested because nested bases are used for the **partial** interaction list of a cluster

algebraic way without storing the entire matrix. The projection-based algebraic nested cross approximation (NCA) was introduced for static problems in [6]. The NCA is a variant of the Adaptive Cross Approximation [5, 26] (from now on abbreviated as ACA) that gives the nested basis for \mathcal{H}^2 matrix. Bebendorf et al. [6] choose indices of points close to the Chebyshev grids and perform ACA upon them to obtain the pivots in a top-bottom fashion, leading to complexity $\mathcal{O}(N \log(N))$. However, [6] required the geometrical information of clusters to find pivots. Zhao et al. [37] develop two purely algebraic NCA algorithms. They first propose an $\mathcal{O}(N \log(N))$ algorithms to find the pivots, which involves a similar approach (top-bottom tree traversal) like [6] but without the geometrical information of clusters. The second algorithm they developed involves a bottom-top tree traversal to find the local pivots followed by a top-bottom tree traversal to find the global pivots. The overall complexity of this algorithm reduces to $\mathcal{O}(N)$. Gujjula et al. [20] proposes a NCA with complexity $\mathcal{O}(N)$, where they show that one can eliminate the second step in [37], i.e., only the bottom-top traversal is sufficient (local pivots are enough), the subsequent top-bottom tree traversal could be redundant (which finds global pivots) without substantial change in the relative error. This makes their NCA slightly computationally faster than the [37]. They also compare their NCA algorithm with [6, 37] and present various benchmarks. We use similar NCAs as in [37, 20] to construct our algorithms, but directly applying them on the *HODLRdD* structure will not produce an **efficient** nested algorithm. This limitation arises because our hierarchical structure (*HODLRdD*) is based on the *weak admissibility condition* [25].

The most important difference between the existing works and ours is that the existing algorithms convert the \mathcal{H} matrix based on the strong/standard admissibility condition to the \mathcal{H}^2 matrix with the same admissibility condition or directly construct the \mathcal{H}^2 matrix. In comparison, this article presents an efficient way to construct the nested version (*nHODLRdD*) of the *HODLRdD* [25] algorithm without using the *HODLRdD* structure, which is based on *weak admissibility condition* [25]. It is by no means a trivial task to construct such a nested hierarchical structure efficiently. We have shown in [25] that weak admissibility-based *HODLRdD* is competitive with the strong admissibility-based \mathcal{H} matrix. This article will investigate whether the *nHODLRdD* is competitive with the algebraic FMM. Also, a semi-nested version (*s-nHODLRdD*) of the *HODLRdD* algorithm is presented in this article.

Main highlights of the article: The following are the main highlights of this article.

1. We present an algebraic fast matrix-vector product algorithm, *nHODLRdD*. We rely on the nested cross approximation (NCA) to build the *nHODLRdD* structure. The construction/initialization cost of the *nHODLRdD* hierarchical structure scales as $\mathcal{O}(pN \log(N))$ and the complexity of the matrix-vector product for non-oscillatory kernels using the *nHODLRdD* structure is $\mathcal{O}(pN)$, p is the maximum rank of the compressed off-diagonal blocks, which grow at most poly logarithmically with N . The numerical results in 2D and 3D ($d = 2, 3$) show that the proposed *nHODLRdD* algorithm is competitive to the algebraic FMM in d dimensions with respect to the matrix-vector product time and space complexity.
2. The second fast matrix-vector product algorithm we develop is the *s-nHODLRdD*, which is a semi-nested variant of the *HODLRdD* algorithm. The construction/initialization cost of the proposed *s-nHODLRdD* hierarchical structure scales as $\mathcal{O}(pN \log(N))$ and the complexity of the matrix-vector product using the *s-nHODLRdD* structure is $\mathcal{O}(pN \log(N))$ for non-oscillatory kernels. Due to the use of semi-nested bases, this algorithm performs better than the *HODLRdD* algorithm (though theoretically, they both have the same asymptotic complexity) in the context of matrix-vector product time and space complexity.
3. We compare the performance of the proposed algorithms (*nHODLRdD*, *s-nHODLRdD*) with two different **algebraic** variants of the FMM and non-nested algorithms like *HODLRdD*, and \mathcal{H} matrix with strong admissibility condition. To be precise, we compare the performance of the two proposed algorithms with 5 different fast matrix-vector product algorithms (Table 7) and present various benchmarks. In 2D, we choose the kernel functions $\log(r)$, $1/r$ and e^{-r} and in 3D, we choose $1/r$, $1/r^4$, e^{ir}/r and Stokes kernel with different distributions (non-uniform and uniform) of particles, where r is the Euclidean distance between source and target.
4. We showcase the applicability of these fast matrix-vector product algorithms by solving integral equations and radial basis function (RBF) interpolation in 2D and 3D using fast iterative solver.

Again, we compare the performance and discuss the scalability of the aforementioned 7 algorithms (Table 7). All the algorithms are implemented in the same fashion using C++ and tested within the same environment, allowing for meaningful comparisons.

5. In the nested algorithms, one of the challenging parts is computing the M2L (multipoles to locals) operations efficiently since it is an expensive part of the nested fast matrix-vector routine. We demonstrate an efficient way to treat the dense M2L operators using the ACA [5].
6. Finally, as a part of this article, we would also like to release the C++ implementation of the proposed $nHODLRdD$ and $s-nHODLRdD$ algorithms made available at <https://github.com/riteshkhan/nHODLRdD/>. Though the repository works for $d = 1, 2, 3$, i.e., for 1D, 2D and 3D problems, we report the results in 2D and 3D since they are more appealing and introduce a new class of hierarchical structures/matrices. It is to be noted that in 1D, $nHODLR1D \equiv HSS \equiv HBS$ and $s-nHODLR1D \equiv HODLR$ (in 1D) $\equiv HODLR1D$.

Outline of the article. The rest of the article is organized as follows. In Section 3, we discuss different hierarchical structures used in this article. The Section 4 discusses the proposed fast algorithms and their analysis. In Section 5, we demonstrate various numerical experiments in 2D and 3D and compare the performance of algebraic nested, semi-nested and non-nested hierarchical matrix algorithms. Further, in Section 6, we present a way to treat the dense M2L operators in nested algorithms efficiently. Finally, we conclude in Section 7.

3. Preliminaries. In this section, we describe the tree data structure used to build the different hierarchical matrix algorithms in this article and briefly discuss two main hierarchical representations used in this article, the $HODLRdD$ [24, 25] and \mathcal{H} matrices [21]. Their performance will be reported later in the Section 5. A brief Nested Cross Approximation (NCA) discussion is also included.

3.1. Construction of the 2^d tree. Let $C \subset \mathbb{R}^d$ be a compact hyper-cube, which contains the N particles. To exploit the hierarchical representations, we need to subdivide the hyper-cube C (computational domain). Depending upon the particle distribution or requirement, one can use different trees like 2^d uniform tree, adaptive 2^d tree, level restricted 2^d tree, K-d tree, etc. But for simplicity, we consider the 2^d uniform tree (for $d = 1, 2$ and 3 , it is binary, quad and oct tree, respectively) in this article. At level 0 of the tree is the hyper-cube C itself (root level). A hyper-cube at a level l is subdivided into 2^d finer hyper-cubes belonging to level $(l + 1)$ of the tree. The former is called the parent of the latter, and the latter (finer hyper-cubes) are the children of the former (coarser hyper-cube). In Figure 1, we illustrate the uniform quad tree at different levels in 2D. We stop the sub-division at a level κ of the tree when each finest hyper-cube contains at most n_{max} particles, where n_{max} is a user-specified threshold that defines the maximum number of particles at each finest hyper-cube. The total $2^{d\kappa}$ finest hyper-cubes at level κ are called the leaves. Note that, $N \leq n_{max} 2^{d\kappa} \implies \kappa = \lceil \log_{2^d} (N/n_{max}) \rceil$.

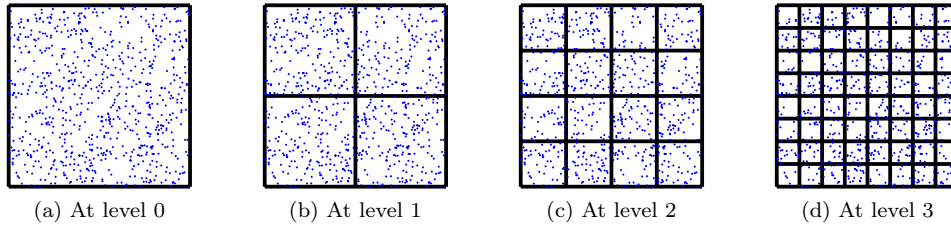


FIG. 1. Hierarchical subdivision of the computational domain C using 2^d uniform tree at different levels ($d = 2$)

3.2. $HODLRdD$ matrix. The article [24] shows that the rank of not just the *far-field* but also the *vertex-sharing* interaction sub-matrices do not scale with any positive power of N for the kernel function $\log(r)$ in 2D and introduce $HODLR2D$ hierarchical structure based on it. The article [25] generalizes this for any non-oscillatory kernel function in d dimensions and proposes that the admissibility of *far-field* and *vertex-sharing* clusters could be considered a way to extend the notion of *weak admissibility* for higher dimensions. The $HODLRdD$ hierarchical structure is based on this proposed *weak admissibility* condition. $HODLRdD$ is a non-nested algorithm with complexity $\mathcal{O}(pN \log(N))$, $p \in \mathcal{O}(\log(N) \log^d(\log(N)))$ [25].

HODLR d admissibility criteria. Two different clusters X and Y at same level l of the 2^d tree are admissible iff either they do not share d' hypersurface ($d' > 0$) or they share at the most a vertex.

Figure 2 illustrates neighbors and the interaction list for a particular cluster C at different levels, and Figure 3 represents the corresponding HODLR2D ($d = 2$) matrices.

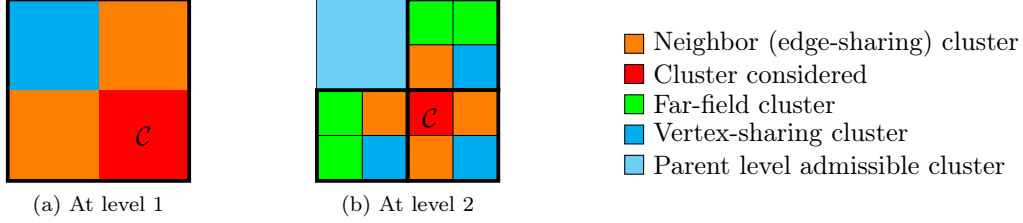


FIG. 2. The neighbors and the interaction list (consist of certain vertex-sharing and far-field clusters) of the cluster C in the HODLR2D at the level 1 and 2 of the quad tree

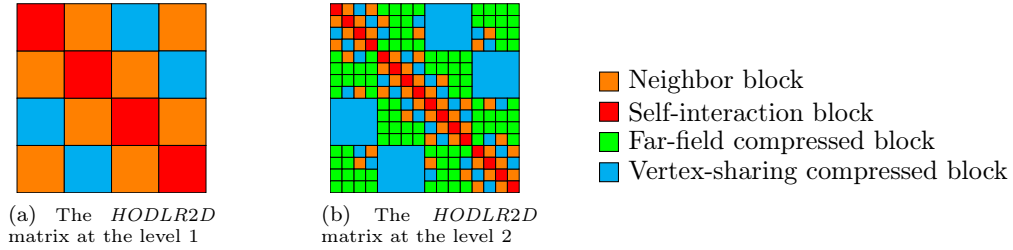


FIG. 3. The HODLR2D matrix at the level 1 and 2

3.3. Standard/strong admissibility \mathcal{H} matrix. The \mathcal{H} -matrix with strong admissibility criteria is the hierarchical low-rank structure whose admissible clusters are the far-field or well-separated clusters.

\mathcal{H} matrix with strong admissibility criteria. Two different clusters X and Y at same level l of the 2^d tree are admissible iff $\max(\text{diam}(X), \text{diam}(Y)) \leq \eta \text{dist}(X, Y)$, where $\text{diam}(X) = \sup\{\|x - y\|_2 : x, y \in X\}$, $\text{dist}(X, Y) = \inf\{\|x - y\|_2 : x \in X, y \in Y\}$ and $\eta = \sqrt{d}$, which holds for $d = 1, 2, 3$. The FMM discussed in this article is based on this strong admissibility criteria. The Figure 4, illustrates neighbors and the interaction list for a particular cluster C at level 2 (Figure 4a) and the corresponding \mathcal{H} matrix with strong admissibility criteria or the FMM matrix (Figure 4b) in 2D.

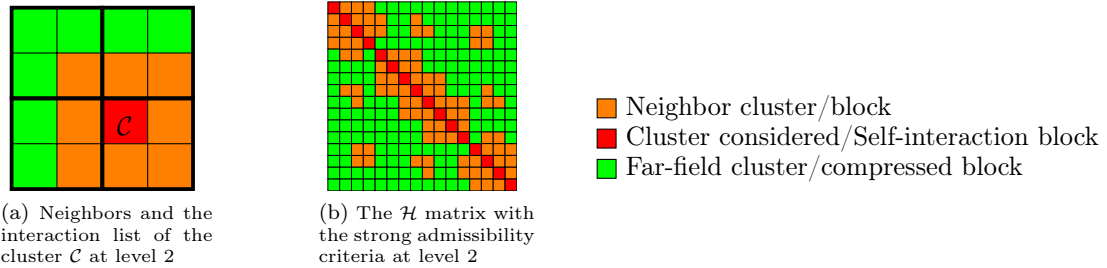


FIG. 4. The neighbors and the interaction list (consist of the far-field clusters) of the cluster C and the \mathcal{H} matrix at the level 2 of the quad tree in 2D (no \mathcal{H} matrix at level 1)

Remark 3.1. The HODLR d D hierarchical structure (Figure 3b) has a couple of advantages over the \mathcal{H} with strong admissibility criteria (Figure 4b).

1. The size of the interaction list of the HODLR d D is smaller than that of the \mathcal{H} matrix (though in the HODLR d D, the sub-matrices corresponding to vertex-sharing interaction possess higher rank than

the far-field interaction rank. However, the vertex-sharing rank does not scale with any positive power of N [25]).

2. The *HODLRdD* performs less number of dense matrix computations than the \mathcal{H} matrix at the leaf level, which is a computationally expensive part.

3.4. The NCA for nested hierarchical structure. Let X and Y be two clusters with global index sets I and J , respectively, such that the cluster Y is in the interaction list of the cluster X , i.e., $Y \in \mathcal{IL}(X)$. The block interaction matrix $K_{I,J}$ can be approximated by ACA [5, 6] as follows:

$$(3.1) \quad K_{I,J} \approx K_{I,J}^{(p)} = UV^* = K_{I,\tau} (K_{\sigma,\tau})^{-1} k_{\sigma,J}$$

where $\sigma \subset I$ and $\tau \subset J$ are called the row and column pivots, respectively. The matrix $K_{I,J}^{(p)}$ is the p^{th} update of the original matrix $K_{I,J}$. Here, we use the partially pivoted ACA algorithm, where for a user-specified tolerance ϵ , the iteration stops if the following condition is true

$$(3.2) \quad \|u_p\|_2 \|v_p\|_2 \leq \epsilon \left\| K_{I,J}^{(p)} \right\|_F$$

where u_p and v_p are the p^{th} column vectors of the matrices U and V , respectively. The ACA-based \mathcal{H} matrix-like fast algorithm leads to a complexity of $\mathcal{O}(N \log(N))$. One needs an algorithm that exploits the nestedness among the admissible clusters to achieve a lower complexity, so the NCA was proposed [6, 37, 20]. The low-rank approximation via NCA takes the form [6]

$$(3.3) \quad K_{I,J} \approx \underbrace{K_{I,\tau_X} (K_{\sigma_X,\tau_X})^{-1}}_{U_X} \underbrace{K_{\sigma_X,\tau_Y}}_{T_{X,Y}} \underbrace{(K_{\sigma_Y,\tau_Y})^{-1} K_{\sigma_Y,J}}_{V_Y^*}$$

where $\sigma_X \subset I$ and $\tau_X \subset \mathcal{AL}(X)$ are the pivots corresponding to X ; $\tau_Y \subset J$ and $\sigma_Y \subset \mathcal{AL}(Y)$ are the pivots corresponding to Y . The notation $\mathcal{AL}(X)$ denotes the union of all the clusters forming the interaction list ($\mathcal{IL}(X)$) at the same level, and the clusters that form the interaction list with X 's ancestors at the lower level of the tree. The U_X and V_Y^* in Equation (3.3) are the column basis of X and the row basis of Y , respectively. To construct the low-rank approximation of the interaction list of a cluster X , we need the matrices U_X and V_Y^*

- If X is a leaf cluster and $Y \in \mathcal{IL}(X)$ then the matrices U_X and V_Y^* are given by

$$(3.4) \quad U_X = K_{I,\tau_X} (K_{\sigma_X,\tau_X})^{-1} \quad \text{and} \quad V_Y^* = (K_{\sigma_Y,\tau_Y})^{-1} K_{\sigma_Y,J}$$

The matrices U_X and V_Y^* are called L2P (local to particles) and P2M (particles to multipole), respectively.

- For a non-leaf cluster $X = \bigcup_{i=1}^{2^d} X_i$, where X_i is a child of X . The matrix U_X is given by

$$(3.5) \quad U_X = \begin{bmatrix} U_{X_1} & 0 & \dots & 0 \\ 0 & U_{X_2} & & 0 \\ \vdots & & \ddots & \vdots \\ 0 & 0 & \dots & U_{X_{2^d}} \end{bmatrix} \begin{bmatrix} \tilde{U}_{X_1 X} \\ \tilde{U}_{X_2 X} \\ \vdots \\ \tilde{U}_{X_{2^d} X} \end{bmatrix}$$

where

$$(3.6) \quad \tilde{U}_{X_i X} = K_{\sigma_{X_i},\tau_X} (K_{\sigma_X,\tau_X})^{-1}, \quad 1 \leq i \leq 2^d$$

The matrices $\tilde{U}_{X_i X}$ are called the L2L (local to local) operators. A similar procedure can be applied to the column clusters to find the M2M (multipole to multipole) operators. The efficiency of NCA hinges on the strategy employed for selecting the pivots that represent the blocks at a specific level of the tree. The validation of NCA, along with numerical error analysis, is presented in [6].

4. Proposed algebraic fast algorithms to calculate the potential. In this section, we begin by showing that the sole application of the NCA with bottom-top pivot selection strategy [37, 20] is not suitable to get a nested hierarchical structure for our weak admissibility-based *HODLRdD* [25] hierarchical structure. Top-bottom pivot selection strategy [6, 37] can be helpful in this case. We then develop a *naive nHODLRdD* nested algorithm based on the NCA with top-bottom pivot selection strategy. After that, we introduce our proposed algorithms: an efficient *nHODLRdD* nested algorithm and a semi-nested variant denoted as *s-nHODLRdD*.

4.1. NCA with bottom-top vs top-bottom pivot selection. The NCA with bottom-top pivot selection [37, 20] is primarily suited for hierarchical structures based on the *strong admissibility criteria* because the admissible clusters are the far-field or the well-separated clusters and the far-field interaction rank remains constant (scales as $\mathcal{O}(1)$). The bottom-top pivot selection strategy is incompatible with our *HODLRdD* hierarchical structure, which is constructed based on a *weak admissibility criteria* (subsection 3.2). In the *HODLRdD* hierarchical structure, the maximum rank of the off-diagonal blocks grows polylogarithmically with N . The bottom-top (B2T) pivot selection selects the leaf clusters' global row and column indices and applies ACA. For non-leaf clusters, it applies ACA upon the clusters' children pivots of the row and column, and the process recursively goes from bottom to top of the tree. Now, we show why the B2T pivot selection is not suitable for the *HODLRdD* hierarchical structure.

We proved in [25] that rank of interaction between two identical d dimensional hyper-cubes containing N uniformly distributed particles and that share a vertex scales as $\mathcal{O}(\log(N) \log^d(\log(N)))$. The admissible clusters of the *HODLRdD* comprise the far-field and vertex-sharing clusters, so the rank scales as $\mathcal{O}(\log(N) \log^d(\log(N)))$ of this structure. The main problem is as we ascend from the bottom to the top of the tree, the size of the simulation cluster (\mathcal{C}) becomes larger. Consequently, the number of particles within the cluster \mathcal{C} , denoted as \mathcal{C}_N , also increases and the vertex-sharing interaction rank grows as $\mathcal{O}(\log(\mathcal{C}_N) \log^d(\log(\mathcal{C}_N)))$. Consider two vertex-sharing admissible leaf clusters containing n_{max} particles. Let R_l be the rank estimate of a vertex-sharing block interaction matrix at a level l of the tree. We will see the effect on the rank of a vertex-sharing admissible clusters if we apply the B2T type pivot selection. At the leaf level, κ , the low-rank approximation (ACA) is applied to the global row and column index sets, and R_κ scales as $\mathcal{O}(\log(n_{max}) \log^d(\log(n_{max})))$. At a non-leaf level, two admissible clusters sharing a vertex can be interpreted as $(2^d - 1)$ far-field clusters at the child level (Figure 5b), with a single vertex-sharing clusters at the child level (Figure 5c) as in Figure 5. Considering \mathcal{F}_l as the rank of interaction between far-field (or well-separated) clusters and \mathcal{V}_l as the rank of interaction between vertex-sharing clusters, the following recurrence relation governs the estimate of R_l at the non-leaf level l .

$$(4.1) \quad R_l \approx (2^d - 1)\mathcal{F}_l + \mathcal{V}_l, \quad l = \kappa - 1 : 1$$

where $\mathcal{F}_l \in \mathcal{O}(1)$ and $\mathcal{V}_l \in \mathcal{O}(\log(2^d R_{l+1}) \log^d(\log(2^d R_{l+1}))) = \mathcal{O}(\log(R_{l+1}) \log^d(\log(R_{l+1})))$. From Equation (4.1), it is clear that as we go to the top of the tree, \mathcal{V}_l scales as a nested “log” expression, which yields a diminutive value. But the actual vertex-sharing rank grows as $\mathcal{O}(\log(N/2^{dl}) \log^d(\log(N/2^{dl})))$ and the term $N/2^{dl}$ increase as l decrease (as we go bottom to top the l decrease). Therefore, if we apply the NCA with B2T pivot selection to the vertex-sharing interaction, the rank's diminutive value is insufficient to get a good approximation of the vertex-sharing interaction block matrix. The interaction list of a cluster may contain multiple vertex-sharing clusters, exacerbating the issue. So, it is clear that only picking the child level pivots in B2T manner is insufficient to get a good nested hierarchical approximation for the weak admissibility-based *HODLRdD* structure.

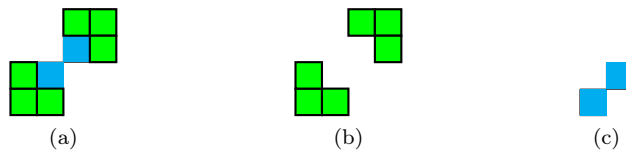


FIG. 5. We can divide the vertex-sharing interaction like above in 2D to get a rank estimate in B2T approach

Hence, we see that the bottom-top pivot selection is **inappropriate** for the *HODLRdD* hierarchical structure or any hierarchical structure where the rank of interaction between two admissible clusters is not constant, leading to a considerable reduction in accuracy (Tables 1 and 2).

On the other hand, in the top-bottom pivot selection [6, 37], ACA is directly applied to the global index sets of the parent less (no parent exists) clusters. Let X be a cluster at a level l of the tree with the parent, and Y is in the interaction list of the cluster X . Then, the row set (I) is formed by taking the global index set of X and the column set (J) is formed by taking the global index set of Y and appending the column pivots of the parent of X (the parent belongs to the level $l - 1$ of the tree). After that, the ACA is applied to the sets I and J . This process recursively goes on from top to bottom of the tree. It does not suffer from the problem associated with the bottom-top approach, as it involves appending the parent level pivots with the admissible cluster's global index set. Hence, the top-bottom pivot selection [37] is suitable for our weak admissibility-based *HODLRdD* structure to construct a nested hierarchical structure. To provide numerical evidence of the effectiveness of the NCA with top-bottom pivot selection, we develop the nested hierarchical structure based on the NCA with T2B pivot selection and compare it with the nested hierarchical structure formed using the NCA with B2T pivot selection. For the numerical experiment, we consider $N = 160000$ particles (same source and target) to be uniformly distributed inside the domain $[-1, 1]^2$ and set the maximum particles at leaf-clusters $n_{max} = 400$. The kernel matrix $K \in \mathbb{R}^{N \times N}$ is formed using the kernel function $1/r$. We then separately apply the NCAs with bottom-top and top-bottom pivot selection on the *HODLRdD* hierarchical structure for different user-specified tolerance to get a nested hierarchical structure. Subsequently, we perform a matrix-vector product by applying a random vector to the nested hierarchical structure and tabulate the maximum rank, minimum rank, and average rank obtained from the NCAs in each level of the tree in Tables 1 and 2. It is evident that NCA with B2T pivot selection algorithm throws a bad relative error. Therefore, B2T pivot selection strategy is not suitable for the *nHODLRdD* nested hierarchical structure.

Level of the tree	Level wise rank in B2T ($\epsilon = 10^{-10}$)			Relative error (norm 2)	Level wise rank in T2B ($\epsilon = 10^{-10}$)			Relative error (norm 2)
	Max. rank	Min. Rank	Avg. rank		Max. Rank	Min. rank	Avg. rank	
1	70	60	63	8.594E-03	102	92	95	1.601E-09
2	154	73	113		234	75	153	
3	155	80	129		222	88	168	
4	147	75	126		187	89	143	
5	139	64	85		150	64	88	

TABLE 1

A comparison between NCA with bottom-top (B2T) and top-bottom (T2B) pivot selection on the *HODLR2D* structure. We set the NCA tolerance $\epsilon = 10^{-10}$. The NCA with B2T pivot selection throws a very bad relative error in the matrix-vector product for the kernel $1/r$.

Level of the tree	Level wise rank in B2T ($\epsilon = 10^{-12}$)			Relative error (norm 2)	Level wise rank in T2B ($\epsilon = 10^{-12}$)			Relative error (norm 2)
	Max. rank	Min. Rank	Avg. rank		Max. Rank	Min. rank	Avg. rank	
1	96	80	86	8.5501E-03	127	114	123	1.1722e-11
2	213	108	158		335	142	218	
3	222	108	182		288	106	226	
4	202	108	167		253	119	185	
5	181	64	97		199	64	99	

TABLE 2

A comparison between NCA with bottom-top (B2T) and top-bottom (T2B) pivot selection on the *HODLR2D* structure. We set the NCA tolerance $\epsilon = 10^{-12}$. The NCA with B2T pivot selection throws a very bad relative error in the matrix-vector product for the kernel $1/r$.

Despite the good accuracy and quasi-linear complexity of the NCA with top-bottom pivot selection, the associated constant in the complexity estimate is very large, leading to a significant time consumption during the numerical experiment.

We demonstrate in Section 5 that the initialization cost of the **naive** *nHODLRdD* based on the only top-bottom (T2B) pivot selection (The *nHOD(t)* algorithm in Table 7) is notably high, indeed the **highest** among all the other algorithms mentioned in Table 7. This renders it less appealing in terms of initialization time. By contrast, NCAs based on the direct application of neither the bottom-top nor the top-bottom pivot selection will yield an **efficient** *nHODLRdD* nested algorithm.

4.2. The proposed efficient $nHODLRdD$ nested algorithm. We introduce some notations in Table 3, which will be used to explain the proposed algorithms. The interaction list and the near-field list of a cluster in the $HODLRdD$ hierarchical structure are also presented in Table 3.

\mathcal{C}	Cluster of particles inside a hyper-cube at a level l of the 2^d tree
$\mathcal{F}(\mathcal{C})$	Set of clusters that are in far-field of \mathcal{C} i.e., hyper-cubes which are at least one hyper-cube away from \mathcal{C} or well-separated from \mathcal{C}
$\mathcal{HS}_{\mathcal{C},d'}$	Set of clusters such that their corresponding hyper-cubes share d' hyper-surface with the hyper-cube corresponding to \mathcal{C} e.g., $\mathcal{HS}_{\mathcal{C},0}$ is the set of clusters such that their hyper-cubes share a vertex with the hyper-cube corresponding to the cluster \mathcal{C}
child(\mathcal{C})	Set of clusters such that their hyper-cubes are children of the coarser hyper-cube corresponding to \mathcal{C}
parent(\mathcal{C})	Set of cluster (at coarser level) with child as \mathcal{C} (at finer level)
siblings(\mathcal{C})	$\text{child}(\text{parent}(\mathcal{C})) \setminus \mathcal{C}$
clan(\mathcal{C})	$\{\text{siblings}(\mathcal{C})\} \cup \{\text{child}(P) : P \in \bigcup_{d'=0}^{d-1} \mathcal{HS}_{\text{parent}(\mathcal{C}),d'}\}$
$\mathcal{IL}(\mathcal{C})$	The interaction list of a cluster \mathcal{C} for the $HODLRdD$ structure is defined as $\text{clan}(\mathcal{C}) \cap (\mathcal{HS}_{\mathcal{C},0} \cup \mathcal{F}_{\mathcal{C}})$
$\mathcal{N}(\mathcal{C})$	The near-field (neighbor+self) list of a cluster \mathcal{C} is defined as $\bigcup_{d'=1}^{d-1} \mathcal{HS}_{\mathcal{C},d'} \cup \mathcal{C}$
n_{max}	Maximum number of particles at leaf-clusters
\tilde{K}	\tilde{K} represent the hierarchical low-rank representation of the original kernel matrix K

TABLE 3
Notations used to describe the $nHODLRdD$ and $s-nHODLRdD$ algorithms

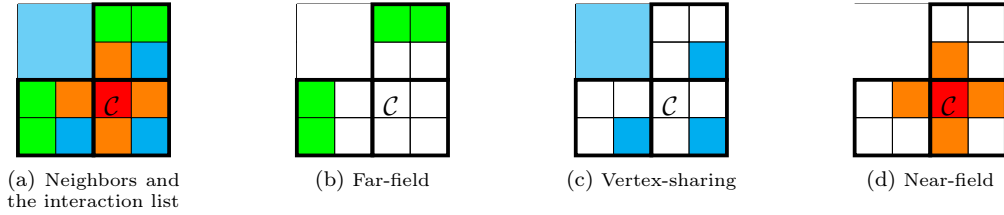


FIG. 6. The neighbors and the interaction list corresponding to cluster \mathcal{C} and its parent with partitioning in 2D

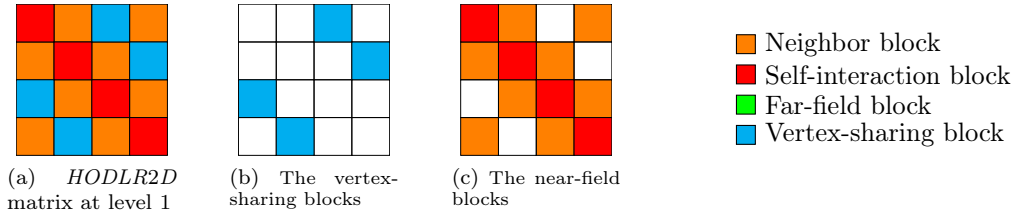


FIG. 7. $HODLR2D$ matrix at level 1 and different interaction block matrices at level 1 (no far-field block matrix at level 1)

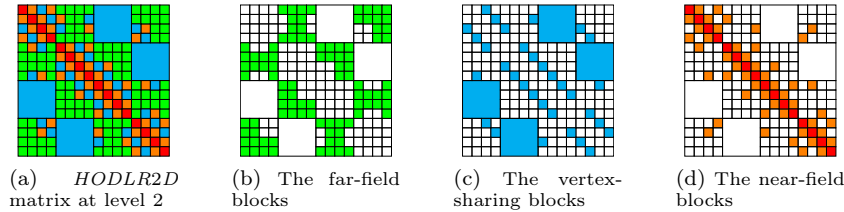


FIG. 8. $HODLR2D$ matrix at level 2 and different interaction block matrices at level 2. The far-field and vertex-sharing blocks are compressed using the NCA with B2T and T2B pivot selection, respectively.

The $HODLRdD$ structure is constructed according to the admissibility criteria outlined in Subsection 3.2. This criterion delineates that **certain** far-field (or well-separated) and vertex-sharing clusters are admissible

clusters. Therefore, the interaction list of a cluster \mathcal{C} consists of both the far-field and vertex-sharing clusters. To construct an efficient $nHODLRdD$ structure we partition the interaction list, $\mathcal{IL}(\mathcal{C})$ into the far-field interaction list denoted as $\mathcal{IL}_{far}(\mathcal{C})$ and the vertex-sharing interaction list denoted as $\mathcal{IL}_{ver}(\mathcal{C})$, i.e., $\mathcal{IL}(\mathcal{C}) = \mathcal{IL}_{far}(\mathcal{C}) \cup \mathcal{IL}_{ver}(\mathcal{C})$. The visual representation of this partitioning is depicted in [Figure 6](#). In our efficient $nHODLRdD$ algorithm, for a cluster \mathcal{C} of the tree, we apply the NCA with bottom to top pivot selection upon the $\mathcal{IL}_{far}(\mathcal{C})$ and the NCA with top to bottom pivot selection upon the $\mathcal{IL}_{ver}(\mathcal{C})$. We need to traverse the tree twice in different directions (bottom-top and top-bottom) with different interaction lists to initialize the $nHODLRdD$ structure. Therefore, we introduce two sets of P2M, M2M, M2L, L2L, and L2P operators: one set for the far-field interactions and another for the vertex-sharing interactions. The initialization steps are described as follows:

1. **Bottom-top pivot selection for far-field interaction.** We have shown that the NCA with B2T pivot selection approach is not appropriate for the entire interaction list of a cluster in our weak admissibility-based hierarchical structure. But if we separate the far-field and the vertex-sharing interaction then we can apply the B2T pivot selection approach only to the far-field interactions associated with a cluster X . The search space for the local pivots is the far-field interaction list $\mathcal{IL}_{far}(X)$ of a cluster X .

- If X is a leaf cluster (child less), then

$$(4.2) \quad \tilde{\sigma}_X := I = \text{global index set of } X \quad \text{and} \quad \tilde{\tau}_X := \bigcup_{Y \in \mathcal{IL}_{far}(X)} \text{global index set of } Y$$

- If X is a non-leaf cluster, then

$$(4.3) \quad \tilde{\sigma}_X := \bigcup_{c \in \text{child}(X)} \sigma_c \quad \text{and} \quad \tilde{\tau}_X := \bigcup_{Y \in \mathcal{IL}_{far}(X)} \bigcup_{c \in \text{child}(Y)} \sigma_c$$

We perform the ACA on the sub-matrix $K_{\tilde{\sigma}_X, \tilde{\tau}_X}$ using a user-given tolerance ϵ_{far} . The set σ_X is the row pivots obtained from the ACA. The detailed procedure is described in [Algorithm 4.1](#). The above sets are the primary components for constructing the operators corresponding to the far-field M2L ($T_{i,j}^{far}$), L2P (U_i^{far}), L2L ($\tilde{U}_{i,j}^{far}$) (Equations (3.3) and (3.6)). The P2M operators (V_i^{far}) or M2M operators ($\tilde{V}_{i,j}^{far}$) can be constructed in a similar fashion.

2. **Top-bottom pivot selection for vertex-sharing interaction.** As demonstrated in [Subsection 4.1](#), the T2B pivot selection can be well-suited for our hierarchical structure. However, instead of applying the T2B pivot selection to the entire interaction list of a cluster X , we employ it solely for the vertex-sharing interactions associated with the cluster X , i.e., only for the $\mathcal{IL}_{ver}(X)$.

- If X has no parent, i.e., $\text{parent}(X) = \text{NULL}$ (parent less), then

$$(4.4) \quad \tilde{\sigma}_X := I = \text{global index set of } X \quad \text{and} \quad \tilde{\tau}_X := \bigcup_{Y \in \mathcal{IL}_{ver}(X)} \text{global index set of } Y$$

- If X has parent, i.e., $\text{parent}(X) \neq \text{NULL}$ then

$$(4.5) \quad \tilde{\sigma}_X := I = \text{global index set of } X \quad \text{and} \quad \tilde{\tau}_X := \bigcup_{Y \in \mathcal{IL}_{ver}(X)} \text{global index set of } Y \quad \bigcup \tau_{\text{parent}(X)}$$

We perform the ACA on the sub-matrix $K_{\tilde{\sigma}_X, \tilde{\tau}_X}$ using a user-given tolerance ϵ_{ver} . The set σ_X is the row pivots obtained from the ACA. The detailed procedure is described in [Algorithm 4.2](#). The above sets are the primary components for constructing the far-field M2L ($T_{i,j}^{ver}$), L2P (U_i^{ver}), L2L ($\tilde{U}_{i,j}^{ver}$) operators (Equations (3.3) and (3.6)). The P2M operators (V_i^{ver}) or M2M operators ($\tilde{V}_{i,j}^{ver}$) can be constructed in a similar fashion.

Remark 4.1. If the kernel matrix (K) is symmetric, the P2M or M2M operators can be obtained simply by taking the transpose of L2P or L2L operators, respectively. However, in this article, we do not take advantage of the symmetry of the matrix K . Instead, we compute the L2P, L2L, P2M, and M2M operators separately.

The pseudocodes outlining the entire initialization of the $nHODLRdD$ hierarchical structure are presented in Algorithms 4.1 and 4.2. The progressive construction of the $nHODLR2D$ structure is illustrated in Figures 7 and 8.

Initialization steps of $nHODLRdD$.

Initialization step I (Algorithm 4.1), Initialization step II (Algorithm 4.2)

Algorithm 4.1 Bottom-top pivot selection for far-field interaction (initialization step I)

```

1: procedure B2TFAR-PIVOT-SELECTION( $\epsilon_{far}$ )
2:   for  $l = \kappa : 2$  do                                      $\triangleright$  Traverse bottom to top
3:     for  $i = 0 : 2^{dl} - 1$  do
4:        $I.clear()$ 
5:        $J.clear()$ 
6:       if  $l \neq \kappa$  then
7:          $I.insert(\sigma_{child(X)})$                           $\triangleright$  For non-leaf cluster add row pivots of the children to  $I$ 
8:         for  $Y \in \mathcal{IL}_{far}(X)$  do
9:            $J.insert(\sigma_{child(Y)})$ 
10:        end for
11:      else
12:         $I = \text{global index set of } X$ 
13:        for  $Y \in \mathcal{IL}_{far}(X)$  do
14:           $J.insert(\text{global index set of } Y)$ 
15:        end for
16:      end if
17:       $(\sigma_X, \tau_X) = \text{ACA}(I, J, \epsilon)$                       $\triangleright$  Perform ACA to index sets  $I, J$  with tolerance  $\epsilon$ 
18:    end for
19:  end for
20: end procedure

```

Algorithm 4.2 Top-bottom pivot selection for vertex-sharing interaction (initialization step II)

```

1: procedure T2BVERTEX-PIVOT-SELECTION( $\epsilon_{ver}$ )
2:   for  $l = 1 : \kappa$  do                                      $\triangleright$  Traverse top to bottom
3:     for  $i = 0 : 2^{dl} - 1$  do
4:        $I = \text{global index set of } X$ 
5:        $J.clear()$ 
6:       for  $Y \in \mathcal{IL}_{ver}(X)$  do
7:          $J.insert(\text{global index set of } Y)$ 
8:         if  $l > 1$  then
9:            $J.insert(\tau_{parent(X)})$                           $\triangleright$  If column pivots of the parent exist, add it to  $J$ 
10:        end if
11:      end for
12:       $(\sigma_X, \tau_X) = \text{ACA}(I, J, \epsilon)$                       $\triangleright$  Perform ACA to index sets  $I, J$  with tolerance  $\epsilon$ 
13:    end for
14:  end for
15: end procedure

```

Compute the potential $\tilde{\phi} = \tilde{K}\mathbf{q}$. All the required operators will be available after completing the initialization steps to compute the potential. We obtain two different sets of P2M, M2M, M2L, L2L, and L2P operators: one corresponding to the far-field interaction and another corresponding to the vertex-sharing interaction. We introduce two sets of variables to keep track of the potential corresponding to the far-field and vertex-sharing interaction. We independently compute the far-field and vertex-sharing potentials and combine them with the near-field potential to obtain the total potential at the leaf level. The vector $q_i^{(\kappa)}$ denotes the charge corresponding to the i^{th} leaf cluster, i.e., $\mathbf{q} = [q_1^{(\kappa)}; q_2^{(\kappa)}; \dots; q_{2^{d\kappa}}^{(\kappa)}]$ (MATLAB notation)

and $\mathcal{C}_i^{(l)}$ denotes the i^{th} cluster at the level l of the tree. The subscripts in the operators correspond to the respective clusters. The subscripts and superscripts in the vectors represent the corresponding cluster and level of the tree, respectively. The procedure to compute the potential is as follows:

1. **Upward traversal:**

- **Particles to multipole (P2M) at leaf level κ** : For all leaf clusters $\mathcal{C}_i^{(\kappa)}$ calculate

$$v_{i, far}^{(\kappa)} = V_i^{far*} q_i^{(\kappa)}, \quad 1 \leq i \leq 2^{d\kappa} \text{ (Far-field)}$$

$$v_{i, ver}^{(\kappa)} = V_i^{ver*} q_i^{(\kappa)}, \quad 1 \leq i \leq 2^{d\kappa} \text{ (Vertex-sharing)}$$
- **Multipole to multipole (M2M) at non-leaf level** : For all non-leaf $\mathcal{C}_i^{(l)}$ clusters calculate

$$v_{i, far}^{(l)} = \sum_{j \in \text{child}(\mathcal{C}_i^{(l)})} \tilde{V}_{i,j}^{far*} v_{j, far}^{(l+1)}, \quad \kappa - 1 \leq l \leq 2 \text{ and } 1 \leq i \leq 2^{dl} \text{ (Far-field)}$$

$$v_{i, ver}^{(l)} = \sum_{j \in \text{child}(\mathcal{C}_i^{(l)})} \tilde{V}_{i,j}^{ver*} v_{j, ver}^{(l+1)}, \quad \kappa - 1 \leq l \leq 1 \text{ and } 1 \leq i \leq 2^{dl} \text{ (Vertex-sharing)}$$

2. **Transverse traversal:**

- **Multipole to local (M2L) at all levels and for all clusters** : For all cluster $\mathcal{C}_i^{(l)}$ across all levels calculate

$$u_{i, far}^{(l)} = \sum_{j \in \mathcal{IL}_{far}(\mathcal{C}_i^{(l)})} T_{i,j}^{far} v_{j, far}^{(l)}, \quad 2 \leq l \leq \kappa \text{ and } 1 \leq i \leq 2^{dl} \text{ (Far-field)}$$

$$u_{i, ver}^{(l)} = \sum_{j \in \mathcal{IL}_{ver}(\mathcal{C}_i^{(l)})} T_{i,j}^{ver} v_{j, ver}^{(l)}, \quad 1 \leq l \leq \kappa \text{ and } 1 \leq i \leq 2^{dl} \text{ (Vertex-sharing)}$$

3. **Downward traversal:**

- **Local to local (L2L) at non-leaf level** : For all non-leaf clusters $\mathcal{C}_i^{(l)}$ calculate

$$u_{i, far}^{(l+1)} := u_{i, far}^{(l+1)} + \tilde{U}_{i,j}^{far} u_{j, far}^{(l)}, \quad 2 \leq l \leq \kappa - 1, \quad 1 \leq i \leq 2^{dl} \text{ and } j \in \text{parent}(\mathcal{C}_i^{(l)}). \text{ (Far-field)}$$

$$u_{i, ver}^{(l+1)} := u_{i, ver}^{(l+1)} + \tilde{U}_{i,j}^{ver} u_{j, ver}^{(l)}, \quad 1 \leq l \leq \kappa - 1, \quad 1 \leq i \leq 2^{dl} \text{ and } j \in \text{parent}(\mathcal{C}_i^{(l)}). \text{ (Vertex-sharing)}$$
- **Local to particles (L2P) at leaf level κ** : For all leaf clusters $\mathcal{C}_i^{(\kappa)}$ calculate

$$\phi_{i, far}^{(\kappa)} = U_i^{far} u_{i, far}^{(\kappa)}, \quad 1 \leq i \leq 2^{d\kappa} \text{ (Far-field)}$$

$$\phi_{i, ver}^{(\kappa)} = U_i^{ver} u_{i, ver}^{(\kappa)}, \quad 1 \leq i \leq 2^{d\kappa} \text{ (Vertex-sharing)}$$

4. **Near-field interaction and the total potential at leaf level:**

- For each leaf cluster $\mathcal{C}_i^{(\kappa)}$, we add the near-field (neighbor+self) potential, which is a direct computation with the far-field and vertex-sharing potential. The final computed potential of a cluster is given by

$$\phi_i^{(\kappa)} = \underbrace{\phi_{i, far}^{(\kappa)}}_{\text{Far-field potential (nested)}} + \underbrace{\phi_{i, ver}^{(\kappa)}}_{\text{Vertex-sharing potential (nested)}} + \underbrace{\sum_{j \in \mathcal{N}(\mathcal{C}_i^{(\kappa)})} K_{i,j} q_j^{(\kappa)}}_{\text{Near-field potential}}, \quad 1 \leq i \leq 2^{d\kappa}.$$

If $\kappa = 1$ then $\phi_{i, far}^{(\kappa)} = 0$.

The computed potential is given by $\tilde{\phi} = [\phi_1^{(\kappa)}; \phi_2^{(\kappa)}; \dots; \phi_{2^{d\kappa}}^{(\kappa)}]$ (MATLAB notation).

4.2.1. Complexity analysis of $nHODLRdD$. We construct the $nHODLRdD$ hierarchical structure in two different (bottom-top and top-bottom) tree traversals. For a particular cluster \mathcal{C} , its far-field interaction $\mathcal{IL}_{far}(\mathcal{C})$ and vertex-sharing interaction $\mathcal{IL}_{ver}(\mathcal{C})$ are compressed using the [Algorithm 4.1](#) and [Algorithm 4.2](#), respectively.

Time complexity. The time complexity of the initialization steps and the potential calculation steps are given below

- **Far-field interaction compression:** Let the leaf cluster size be bounded by p_1 and we also assume $p_1 = \mathcal{O}(n_{max})$. Let c_{far} be the maximum of the far-field interaction list size of a cluster (in 2D and 3D for the $nHODLRdD$ hierarchical structure $c_{far} = 12$ and 126, respectively). For a non-leaf cluster, we choose the row indices from the row pivots of the children clusters and column indices from the column pivots of the children of the admissible far-field blocks. After that, the partially

pivoted ACA [5] is applied to the row and column indices. The cost for applying ACA for a non-leaf cluster at level l is bounded by $(2^d p_1 + c_{far} 2^d p_1) p_1^2$. By taking all the levels, the cost for the far-field

compression is bounded by $\sum_{l=2}^{\kappa} 2^{dl} (2^d p_1 + c_{far} 2^d p_1) p_1^2 \approx \mathcal{O}(N)$.

- *Vertex-sharing interaction compression:* Let c_{ver} be the maximum of the vertex-sharing interaction list size of a cluster (in 2D and 3D for the $nHODLRdD$ hierarchical structure $c_{ver} = 3$ and 7, respectively). For a cluster (with a parent), we choose the row indices from its index set and column indices from its index set, along with column pivots of the parent of the admissible vertex-sharing blocks. After that, the partially pivoted ACA [5] is applied to the row and column indices. Let p_2 be the maximum size of parent level pivots across the tree to be added, where p_2 scales at most poly logarithmically with N . Then the cost for applying ACA for a particular cluster is bounded by $\left(\frac{N}{2^{dl}} + c_{ver} \frac{N}{2^{dl}} + p_2\right) p_2^2$. By taking all the levels, the cost for the vertex-sharing

interaction compression is bounded by $\sum_{l=1}^{\kappa} 2^{dl} \left(\frac{N}{2^{dl}} + c_{ver} \frac{N}{2^{dl}} + p_2\right) p_2^2 = \sum_{l=1}^{\kappa} (N + c_{ver} N + p_2) p_2^2 \approx \mathcal{O}(p_2 N \log(N))$.

Therefore, the overall time complexity to initialize the $nHODLRdD$ hierarchical structure asymptotically scales as $\mathcal{O}(N + p_2 N \log(N))$. The time required for each step in the potential calculation (subsection 4.2) exhibits a quasi-linear scaling. Therefore, the overall time complexity for the potential calculation scales at most quasi-linearly for non-oscillatory kernels. The step-by-step costs, along with a comparison of algebraic FMM costs, are presented in Table 4.

Space complexity. For a cluster \mathcal{C} at a level l of the tree, we store the different set column basis (L2L operator), row basis (M2M operator), and M2L operators. Total cost for storing the M2M, M2L and L2L operators is $\mathcal{O}(N p_1^2 + N p_2^2)$. The cost of storing the dense near-field operators at leaf level is $\mathcal{O}(N n_{max}^2)$. Therefore, the overall memory cost scales at most quasi-linearly.

STEP	2D ($d = 2$)		3D ($d = 3$)	
	$nHODLR2D$	FMM2D	$nHODLR3D$	FMM3D
P2M+M2M	$\mathcal{O}(N p_1^2 + N p_2^2)$	$\mathcal{O}(N p^2)$	$\mathcal{O}(N p_1^2 + N p_2^2)$	$\mathcal{O}(N p^2)$
M2L	$\mathcal{O}(12N p_1^2 + 3N p_2^2)$	$\mathcal{O}(27N p^2)$	$\mathcal{O}(126N p_1^2 + 7N p_2^2)$	$\mathcal{O}(189N p^2)$
L2L+L2P	$\mathcal{O}(N p_1^2 + N p_2^2)$	$\mathcal{O}(N p^2)$	$\mathcal{O}(N p_1^2 + N p_2^2)$	$\mathcal{O}(N p^2)$
Near-field	$\mathcal{O}(5N n_{max}^2)$	$\mathcal{O}(9N n_{max}^2)$	$\mathcal{O}(19N n_{max}^2)$	$\mathcal{O}(27N n_{max}^2)$

TABLE 4

Comparing the complexities of $HODLRdD$ and algebraic $FMMdD$ for $d = 2$ and $d = 3$. p_1 and p roughly scales as $\mathcal{O}(1)$ but p_2 scales at most poly logarithmically with N .

4.3. The proposed s - $nHODLRdD$ semi-nested algorithm. The s - $nHODLRdD$ is a semi-nested (partially nested, not completely nested) algorithm because we employ both the nested and non-nested bases in this algorithm. Let \mathcal{C} be a cluster at a level l of the tree. The interaction list of \mathcal{C} consists of certain far-field and vertex-sharing interactions and the interaction list can be partitioned, i.e., $\mathcal{IL}(\mathcal{C}) = \mathcal{IL}_{far}(\mathcal{C}) \cup \mathcal{IL}_{ver}(\mathcal{C})$. The far-field interactions ($\mathcal{IL}_{far}(\mathcal{C})$) are compressed using the NCA with bottom-top pivot selection (Algorithm 4.1). The far-field interaction compression routine is the same as the previous $nHODLRdD$ algorithm. The vertex-sharing interactions ($\mathcal{IL}_{ver}(\mathcal{C})$) are compressed using pure ACA (Algorithm 4.3). The ACA is applied to the global row index set and the global column index set associated with the vertex-sharing interaction; there is no dependency between the pivots at the child level and those at the parent level, or vice versa. The vertex-sharing compression routine is the main difference between the $nHODLRdD$ and the s - $nHODLRdD$. In the s - $nHODLRdD$ algorithm, the potential corresponding to the far-field interaction is obtained through a \mathcal{H}^2 matrix-like algorithm, while the potential corresponding to the vertex-sharing interaction is derived using a \mathcal{H} matrix-like algorithm.

To initialize the s - $nHODLRdD$ hierarchical structure, the first step is analogous to the $nHODLRdD$ initialization algorithm, where we employ the Algorithm 4.1 to the far-field interactions. In the second step, we apply Algorithm 4.3 to the vertex-sharing interactions.

Initialization steps of s - $nHODLRdD$ structure.

Initialization step I (Algorithm 4.1), Initialization step II (Algorithm 4.3)

Algorithm 4.3 Compression of the vertex-sharing interaction using only ACA (initialization step II)

```

1: procedure VERTEX-SHARING-INTERACTION-COMPRESSION( $\epsilon_{ver}$ )
2:   for  $l = 1 : \kappa$  do
3:     for  $i = 0 : 2^{dl} - 1$  do
4:        $I = \text{global index set of } X$ 
5:        $J.\text{clear}()$ 
6:       for  $Y \in \mathcal{IL}_{ver}(X)$  do
7:          $J.\text{insert}(\text{global index set of } Y)$ 
8:       end for
9:        $(\sigma_X, \tau_X) = \text{ACA}(I, J, \epsilon)$   $\triangleright$  Perform ACA to index sets  $I, J$  with tolerance  $\epsilon$ 
10:    end for
11:  end for
12: end procedure

```

Compute the potential $\tilde{\phi} = \tilde{K}q$. The far-field potential $\phi_{i, far}^{(\kappa)}$ is computed using the M2M, M2L, and L2L steps, following the same procedure as discussed in the far-field potential calculation of the previous $nHODLRdD$ algorithm (subsection 4.2). The computation of the vertex-sharing potential $\phi_{i, ver}^{(\kappa)}$ is executed in a manner analogous to the \mathcal{H} matrix algorithm, as described in Algorithm 4.4.

Algorithm 4.4 Compute vertex-sharing potential in s - $nHODLRdD$

```

1: procedure VERTEX-SHARING POTENTIAL( $\phi_{ver}$ )
2:   for  $l = 1 : \kappa$  do  $\triangleright$  Low-rank matrix-vector product in non-nested manner
3:     for  $i = 1 : 2^{dl}$  do
4:        $I = \text{global index set of } \mathcal{C}_i^{(l)}$ 
5:       for  $Y \in \mathcal{IL}_{ver}(\mathcal{C}_i^{(l)})$  do
6:          $J = \text{global index set of } Y$ 
7:          $\phi_{i, ver}^{(l)} := \phi_{i, ver}^{(l)} + U(V^* q_j^{(l)})$ 
8:       end for
9:     end for
10:  end for
11:  return  $\phi_{ver}$ 
12: end procedure

```

For each leaf cluster $\mathcal{C}_i^{(\kappa)}$, we add the near-field (neighbor+self) potential, which is a direct computation with the far-field and vertex-sharing potential. The final computed potential of a cluster is given by

$$\phi_i^{(\kappa)} = \underbrace{\phi_{i, far}^{(\kappa)}}_{\text{Far-field potential (nested)}} + \underbrace{\phi_{i, ver}^{(\kappa)}}_{\text{Vertex-sharing potential (non-nested)}} + \underbrace{\sum_{j \in \mathcal{N}(\mathcal{C}_i^{(\kappa)})} K_{i,j} q_j^{(\kappa)}}_{\text{Near-field potential (direct)}}, \quad 1 \leq i \leq 2^{d\kappa}.$$

If $\kappa = 1$ then $\phi_{i, far}^{(\kappa)} = 0$. The computed potential is given by $\tilde{\phi} = [\phi_1^{(\kappa)}; \phi_2^{(\kappa)}; \dots; \phi_{2^{d\kappa}}^{(\kappa)}]$ (MATLAB notation).

4.3.1. Complexity analysis of s - $nHODLRdD$. We construct the s - $nHODLRdD$ hierarchical structure using NCA with B2T pivot selection and the ACA.

Time complexity. The time complexity of the initialization steps and the potential calculation steps are given below

- *Far-field interaction compression:* The far-field compression cost of this algorithm is the same as the $nHODLRdD$ algorithm. Let the leaf cluster size be bounded by p_1 , and we also assume $p_1 = \mathcal{O}(n_{max})$. Let c_{far} be the maximum of the far-field interaction list size (in 2D and 3D for the $nHODLRdD$ hierarchical structure $c_{far} = 12$ and 126, respectively). Considering all the levels, the

cost is bounded by $\sum_{l=2}^{\kappa} 2^{dl} (2^d p_1 + c_{far} 2^d p_1) p_1^2 \approx \mathcal{O}(N)$.

- *Vertex-sharing interaction compression:* Let c_{ver} be the maximum of the vertex-sharing interaction list size of a cluster (in 2D and 3D for the $nHODLRdD$ hierarchical structure $c_{ver} = 3$ and 7, respectively). The partially pivoted ACA [5] is applied to a cluster's global row and column indices. Let p_3 be the maximum rank (vertex-sharing blocks) and $p_3 \in \mathcal{O}(\log(N) \log^d(\log(N)))$ [25]. Then the cost for applying ACA for a particular cluster is bounded by $\left(\frac{N}{2^{dl}} + c_{ver} \frac{N}{2^{dl}}\right) p_3^2$.

By taking all the levels, the cost for the vertex-sharing interaction compression is bounded by $\sum_{l=1}^{\kappa} 2^{dl} \left(\frac{N}{2^{dl}} + c_{ver} \frac{N}{2^{dl}}\right) p_3^2 = \sum_{l=1}^{\kappa} (N + c_{ver} N) p_3^2 \approx \mathcal{O}(p_3 N \log(N))$.

Therefore, the overall time complexity to initialize the s - $nHODLRdD$ hierarchical structure scales asymptotically $\mathcal{O}(N + p_3 N \log(N))$, $p_3 \in \mathcal{O}(\log(N) \log^d(\log(N)))$ [25]. The time required to compute the far-field and vertex-sharing potential calculation exhibits a scaling of $\mathcal{O}(N)$ and $\mathcal{O}(p_3 N \log(N))$, respectively. Therefore, the overall time complexity for potential calculation scales quasi-linearly for the non-oscillatory kernels. **Space complexity.** The cost of storing the far-field M2M, M2L and L2L operators is $\mathcal{O}(N)$, same as shown in the $nHODLRdD$ algorithm. The cost of storing the vertex-sharing U and V operators is roughly $\mathcal{O}(p_3 N \log(N))$. So, the overall storage cost of the s - $nHODLRdD$ algorithm scales quasi-linearly.

Remark 4.2. Note that the compression routines of the far-field and vertex-sharing interactions are distinct and operate independently for both the proposed algorithms. Hence, one has the flexibility to opt for different values of ϵ_{far} and ϵ_{ver} to achieve improved compression and, consequently, enhanced relative error control. However, we set $\epsilon_{far} = \epsilon_{ver}$ throughout this article.

Remark 4.3. Despite having the same asymptotic complexities as the $HODLRdD$ algorithm [25], the proposed s - $nHODLRdD$ algorithm demonstrates improved time and storage efficiency due to using partially nested bases. This enhancement is illustrated in Section 5.

Remark 4.4. It is to be noted that in 1D, $nHODLR1D \equiv HSS \equiv HBS$ and s - $nHODLR1D \equiv HODLR$ (in 1D) $\equiv HODLR1D$.

4.4. Comparison between the proposed algorithms and the algebraic FMM. We compare the proposed algorithms and the algebraic FMM, implemented using the NCA with the bottom-top pivot selection, in terms of memory (total storage to store the hierarchical low-rank representation. Refer Table 8) and relative error in matrix-vector product for the kernel matrix (K) derived from the kernel functions $\log(r)$ in 2D and $1/r$ in 3D. For this experiment, we consider N points uniformly distributed (same source and target) inside the hyper-cube $[-1, 1]^d$, $d \in \{2, 3\}$.

N	ACA/NCA Tolerance = 10^{-08}						ACA/NCA Tolerance = 10^{-10}					
	Memory (GB)			Relative error (norm 2)			Memory (GB)			Relative error (norm 2)		
	$nHODLR2D$	FMM2D	s - $nHODLR2D$	$nHODLR2D$	FMM2D	s - $nHODLR2D$	$nHODLR2D$	FMM2D	s - $nHODLR2D$	$nHODLR2D$	FMM2D	s - $nHODLR2D$
6400	0.0826074	0.103297	0.0856223	5.17E-08	1.60E-08	1.89E-08	0.0843852	0.104339	0.0880307	2.45E-10	1.42E-10	1.80E-10
10000	0.0783573	0.0961874	0.0961874	1.30E-07	4.12E-08	2.57E-08	0.0837643	0.10033	0.095856	1.15E-09	6.21E-10	8.61E-10
40000	0.403955	0.520042	0.480014	4.13E-07	1.43E-07	1.09E-07	0.433689	0.544332	0.526158	3.08E-09	1.76E-09	1.63E-09
90000	1.77145	2.40477	1.97104	3.79E-07	1.87E-07	2.87E-07	1.82801	2.44206	2.0699	7.48E-09	1.79E-09	1.15E-09
160000	1.97815	2.63349	2.4707	5.43E-06	1.08E-06	1.12E-06	2.12602	2.7507	2.70466	4.73E-08	1.18E-08	1.00E-08
250000	4.44415	6.05333	5.27246	3.38E-06	4.96E-07	3.93E-07	4.64201	6.2071	5.64221	2.32E-08	9.64E-09	1.55E-08

TABLE 5

Comparison between the proposed algorithms and algebraic FMM for different tolerance considering the kernel $\log(r)$ in 2D

N	ACA/NCA Tolerance = 10^{-08}						ACA/NCA Tolerance = 10^{-10}					
	Memory (GB)			Relative error (norm 2)			Memory (GB)			Relative error (norm 2)		
	$nHODLR3D$	FMM3D	s - $nHODLR3D$	$nHODLR3D$	FMM3D	s - $nHODLR3D$	$nHODLR3D$	FMM3D	s - $nHODLR3D$	$nHODLR3D$	FMM3D	s - $nHODLR3D$
27000	1.35553	1.47618	1.40219	1.99E-08	1.78E-08	1.80E-08	1.74219	1.88664	1.80435	2.83E-10	1.62E-10	2.51E-10
42875	2.12957	2.31454	2.2831	7.19E-08	5.61E-08	9.15E-08	3.05877	3.30355	3.24056	1.04E-09	6.05E-10	3.99E-09
64000	3.65533	4.06652	3.93143	7.02E-08	7.24E-08	6.65E-08	5.13845	5.65626	5.48342	9.22E-10	1.47E-09	1.20E-08
91125	5.84191	6.61321	6.2449	1.28E-07	1.00E-07	1.18E-07	8.03262	8.89929	8.60427	2.89E-09	2.55E-09	2.83E-09
125000	8.90607	10.0255	9.50777	1.01E-07	1.09E-07	8.56E-08	11.9944	13.347	12.8275	2.22E-09	1.39E-09	2.11E-09
216000	19.4068	21.9217	20.535	2.30E-07	2.71E-07	2.35E-07	26.1176	29.5915	27.6902	1.74E-09	1.95E-09	1.60E-09

TABLE 6

Comparison between the proposed algorithms and algebraic FMM for different tolerance considering the kernel $1/r$ in 3D

5. Numerical results. This section presents various numerical experiments to demonstrate the effectiveness of the proposed algorithms. We also compare various benchmarks of the proposed algorithms with other existing algebraic fast algorithms. For convenience, we introduce a few notations in Table 7 corresponding to the 7 different fast algorithms whose performance will be reported in this section. We perform the following experiments in 2D and 3D for all the 7 algorithms as in Table 7, report their performance, scalability, and plot various benchmarks.

- (1) Fast Matrix-vector product for the kernel matrix arises from different kernel functions and different distributions (uniform and non-uniform) of particles.
- (2) Fast iterative solver (GMRES) for a system, where non-diagonal entries of the system matrix arise from the Helmholtz kernel with wavenumber set to 1.
- (3) Fast iterative solver (GMRES) for RBF interpolation.
- (4) Fast iterative solver (GMRES) for the Fredholm integral equation of the second kind.

$nHOD(b+t)$	The proposed $nHODLRdD$ algorithm in this article, where we use NCA with B2T (Algorithm 4.1) and T2B (Algorithm 4.2) pivot selection for far-field and vertex-sharing interaction, respectively. (<i>nested algorithm</i>)
$FMM(b)$	The algebraic FMM algorithm, where we only use NCA with B2T for pivot selection. (<i>nested algorithm</i>)
$s-nHOD$	The proposed $s-nHODLRdD$ in this article, where we use NCA with B2T pivot selection for far-field and pure ACA for vertex-sharing interaction. We use both nested and non-nested techniques in this algorithm. (<i>semi-nested algorithm</i>)
$nHOD(t)$	The <i>naive</i> nested $HODLRdD$ algorithm, where we only use NCA with T2B pivot selection. (<i>nested algorithm</i>)
$FMM(t)$	The algebraic FMM algorithm, where we only use NCA with T2B pivot selection. (<i>nested algorithm</i>)
HOD	The $HODLRdD$ algorithm, based on our proposed <i>weak admissibility</i> criteria [25]. (<i>non-nested algorithm</i>)
\mathcal{H}	The \mathcal{H} matrix algorithm with strong/standard admissibility condition (subsection 3.3). (<i>non-nested algorithm</i>)

TABLE 7
Notations for the seven different fast matrix-vector product algorithms in this article

The notation $b+t$ signifies the utilization of both the bottom-top and top-bottom pivot selection strategies. On the other hand, b or t denotes the exclusive application of either bottom-top or top-bottom pivot selection strategy, respectively. We tabulated the performance of all the 7 algorithms (Table 7) in each experiment. The column corresponding to the best or worst perform algorithm (in terms of time or memory) is highlighted in cyan or red, respectively. The job either exceeds the specified wall time or is out of the memory corresponding to the cells with “–” in the tables.

All the algorithms are implemented in C++ and performed on an Intel Xeon Gold 2.5GHz processor with the same environment setup. Except for the first type experiments, i.e., the Item (1) (no solver is involved), in all the remaining types experiments, i.e., the Items (2) to (4), we parallelize only the fast matrix-vector product routine as a part of the GMRES [30] routine with 8 OpenMP threads. Since we compare nested, semi-nested, and non-nested algorithms, **we do not parallelize the initialization routine of any experiment in this article**. Further, we introduce some notations in Table 8, which are used in this section.

N	Total number of particles (we consider the same source and target) in the domain
Initialization Time	The entire time taken (in seconds) to create the hierarchical low-rank representation (Initialization routine) including the time to assemble different operators/matrices. This refers to the overall execution time, excluding the time spent on the matrix-vector product operation.
K	K represent the hierarchical low-rank representation of the original kernel matrix K
MVP time	The time taken (in seconds) to compute the matrix-vector product using the low-rank representation
Memory	The total memory (in GB) needed to store the hierarchical low-rank representation (K) without exploiting the symmetric property of K .
Solution time	Total time (in seconds) to solve the system $K\sigma = f$ using the fast iterative solver. We use GMRES [30] in our experiments. In the GMRES routine, the matrix-vector product is accelerated using the hierarchical low-rank representation (K)
n_{max}	Maximum number of particles in leaf level cluster. We set $n_{max} = 400$ and 512 for the experiments in 2D and 3D, respectively
Relative error in matrix-vector product	Let q be a random column vector and the exact matrix-vector product $\phi = Kq$ (exact up to round-off). The computed column vector $\hat{\phi}$ is given by $\hat{\phi} = Kq$. The norm 2 relative error in the matrix-vector product is given by $\ \hat{\phi} - \phi\ _2 / \ \phi\ _2$
Relative error in solution	Let q be a random column vector and the exact matrix-vector product $b = Kq$ (exact up to round-off). We set b as RHS and solve the system $K\lambda = b$ using the iterative solver, GMRES. The norm 2 relative error in the solution of the system is given by $\ \lambda - q\ _2 / \ q\ _2$
NCA/ACA tolerance	The NCA/ACA tolerance is set $\epsilon = \epsilon_{near} = \epsilon_{far} = 10^{-12}$ and 10^{-7} for all the experiments in 2D and 3D, respectively
GMRES stopping condition	We use GMRES [30] without restart, and GMRES routine will terminate if the relative residual is less than ϵ_{GMRES} . The matrix-vector product part in the GMRES routine is accelerated using fast matrix-vector product algorithms (Table 7) and OpenMP enabled in the fast matrix-vector product routine. We set $\epsilon_{GMRES} = 10^{-12}$ and 10^{-10} for the experiments in 2D and 3D, respectively
$\#iter$	The number of iterations of the iterative solver (GMRES), where the matrix-vector product is accelerated with the proposed $nHOD(b+t)$. The number of iterations is almost the same (1 iteration more or less) for the other fast matrix-vector algorithms (Table 7) accelerated GMRES

TABLE 8
Notations that are used in this section

Remark 5.1. The NCA with bottom-top or top-bottom pivot selection are both applicable for the FMM structure [37]. In Table 7, $FMM(b)$ and $FMM(t)$ denote the FMM is implemented using the NCA with bottom-top and top-bottom pivot selection, respectively. But in Subsection 4.1, we have shown that the bottom-top pivot selection strategy is unsuitable for the entire interaction list of the $nHODLRdD$ structure.

Remark 5.2. In this article, all the nested hierarchical structures ($nHODLRdD$, $FMMdD$) take into account the storage calculation associated with the M2M, L2L and all the M2L operators. We use this approach because the non-nested algorithms used in this article do not take advantage of the kernel matrix's symmetric property. To ensure consistency and uniformity, this approach is adopted. But for a symmetric kernel matrix, the M2M and L2L operators are transposes of one another, so we do not need to store them together. In a word, the storage and initialization cost can be further reduced by roughly a factor of 2 by exploiting the symmetric property of the kernel matrix.

5.1. Experiments in two dimensions. In this subsection, we perform various experiments in 2D. We consider N overlapping source and target points for all the experiments.

5.1.1. Fast matrix-vector product in 2D. Below, we report the results for three different kernel functions (the first two are singular, and the last one is non-singular) on the different distributions of the location of particles $\{\mathbf{x}_i\}_{i=1}^N$.

1. $F(r) = \log(r)$ (single layer Laplacian in 2D) Table 9, Table 10 and Figure 9
2. $F(r) = 1/r$ Table 11, Table 12 and Figure 10
3. $F(r) = e^{-r}$ (Matérn kernel) Table 13, Table 14 and Figure 11

where r is the Euclidean distance between source and target points, i.e., $r = \|\mathbf{x}_i - \mathbf{x}_j\|_2$. The $(i, j)^{th}$ entry of the kernel matrix K arises from the singular kernel function is given by

$$(5.1) \quad K(i, j) = \begin{cases} F(r) = F(\|\mathbf{x}_i - \mathbf{x}_j\|_2) & \text{if } i \neq j \\ 0 & \text{otherwise} \end{cases}$$

The $(i, j)^{th}$ entry of the kernel matrix K arises from the non-singular kernel function is given by $K(i, j) = F(r) = F(\|\mathbf{x}_i - \mathbf{x}_j\|_2)$. For the first two kernel functions, $\log(r)$ and $1/r$, we consider the N overlapping source and target as the $\sqrt{N} \times \sqrt{N}$ Chebyshev grid on $[-1, 1]^2$ and we choose N random uniformly distributed overlapping source and target on $[-1, 1]^2$ for the last kernel function (e^{-r}). We take 5 different column vectors ϕ and tabulate the average initialization time, MVP time, memory and relative error of all the seven fast matrix-vector algorithms (as mentioned in Table 7) in Tables 9 to 14. In Figures 9 to 11, we plot the scaling of the initialization time, average MVP time and memory for the algorithms $nHOD(b+t)$, $FMM(b)$ and $s-nHOD$ (as mentioned in Table 7).

Experiment 1.

N	Initialization time (s)							MVP time (s)						
	$nHOD(b+t)$	$FMM(b)$	$s-nHOD$	$nHOD(t)$	$FMM(t)$	HOD	\mathcal{H}	$nHOD(b+t)$	$FMM(b)$	$s-nHOD$	$nHOD(t)$	$FMM(t)$	HOD	\mathcal{H}
10000	1.41	1.37	1.4	2.05	1.72	1.73	1.88	0.01	0.01	0.01	0.01	0.01	0.01	0.02
40000	8.39	7.79	7.91	16.93	12.15	8.68	12.35	0.03	0.03	0.05	0.03	0.05	0.04	0.1
90000	22.11	24.82	24.1	48.49	36.48	31.06	35.48	0.06	0.15	0.15	0.07	0.15	0.26	0.21
160000	48.25	39.51	42.94	121.7	77.74	49.92	73.11	0.14	0.18	0.2	0.15	0.16	0.29	0.38
250000	92.22	71.79	76.56	198.08	133.66	111.07	123.66	0.28	0.39	0.39	0.32	0.4	0.62	0.61
490000	203.78	139.23	163.88	501.3	309.69	257.89	282.1	0.37	0.53	0.89	0.42	0.48	1.21	1.18
1000000	485.89	349.74	410.84	1372.15	781.98	494.03	731.21	1.1	2.2	2.54	1.64	1.95	4.1	4.41
2250000	1338.79	779.11	1005.31	3419.92	2226.64	1413.54	1694.65	2.11	4.69	5.01	2.22	3.83	7.56	8.79
4000000	2764.34	1578.87	2063.23	9245.78	4310.59	2880.02	3395.02	7.38	11.35	11.97	8.48	10.49	18.19	21.22
6250000	4503.45	3361.32	3705.95	12457.2	7138.59	5164.72	6407.24	12.11	22.54	23.11	15.44	22.78	38.06	42.96

TABLE 9

Time comparison of the algorithms as mentioned in Table 7 for the kernel function $\log(r)$

N	Memory (GB)							Relative error in matrix-vector product (norm 2)						
	nHOD(b+t)	FMM(b)	s-nHOD	nHOD(t)	FMM(t)	HOD	\mathcal{H}	nHOD(b+t)	FMM(b)	s-nHOD	nHOD(t)	FMM(t)	HOD	\mathcal{H}
10000	0.0904	0.1055	0.1043	0.0903	0.1055	0.1429	0.1708	5.20E-12	1.09E-12	3.89E-12	2.53E-11	5.71E-12	5.81E-13	3.74E-13
40000	0.4678	0.5759	0.5713	0.4810	0.5749	0.8446	1.0463	7.60E-12	5.24E-11	3.05E-12	9.65E-11	1.84E-11	6.81E-12	7.96E-13
90000	1.8815	2.5775	2.1618	1.8869	2.4872	2.81	3.6141	2.82E-10	3.92E-11	5.03E-11	1.41E-09	4.33E-11	5.84E-12	4.05E-13
160000	2.2820	2.8993	2.9613	2.3921	2.8942	4.59	5.7870	3.02E-10	2.26E-10	9.72E-11	2.75E-09	1.89E-10	7.09E-12	1.11E-12
250000	4.8476	6.3858	5.9896	4.9550	6.3812	8.60	11.0308	4.01E-10	8.46E-11	1.53E-10	1.16E-09	1.02E-10	4.24E-11	1.31E-12
490000	7.1254	9.0870	10.0367	7.6029	9.0692	16.6499	21.0888	4.92E-10	1.40E-10	2.14E-10	2.70E-09	6.57E-10	1.32E-11	1.17E-12
1000000	23.393	31.8277	30.063	23.9924	31.8001	44.1237	57.4261	1.14E-09	3.20E-10	1.79E-10	1.34E-08	1.90E-09	2.10E-10	1.19E-11
2250000	41.127	54.5982	59.765	43.5994	54.5118	98.9377	127.003	2.35E-09	1.79E-09	2.46E-10	-	-	-	-
4000000	110.83	154.835	146.975	113.615	154.728	218.425	287.218	-	-	-	-	-	-	-
6250000	252.64	362.267	312.673	255.443	362.157	426.184	572.844	-	-	-	-	-	-	-

TABLE 10

Memory and relative error ($\epsilon = 10^{-12}$) of the algorithms as mentioned in Table 7 for the kernel function $\log(r)$

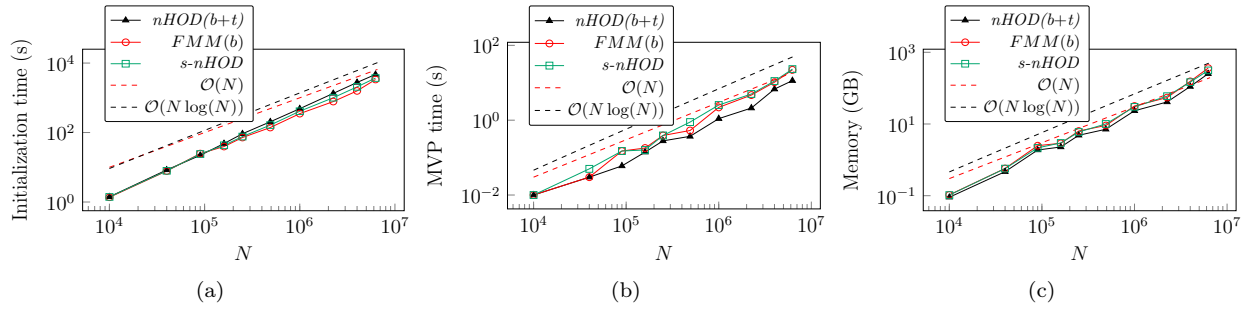


FIG. 9. Plots of initialization time (Figure 9a), MVP time (Figure 9b) and memory (Figure 9c) for $\log(r)$

Experiment 2.

N	Initialization time (s)							MVP time (s)						
	nHOD(b+t)	FMM(b)	s-nHOD	nHOD(t)	FMM(t)	HOD	\mathcal{H}	nHOD(b+t)	FMM(b)	s-nHOD	nHOD(t)	FMM(t)	HOD	\mathcal{H}
10000	2.36	2.3	2.02	4.08	2.49	1.73	1.48	0.01	0.01	0.01	0.01	0.01	0.02	0.04
40000	20.59	15.39	14.45	49.18	22.51	12.51	10.93	0.03	0.03	0.03	0.03	0.07	0.04	0.12
90000	61.67	36.1	38.29	170.37	65.71	33.44	28.33	0.1	0.12	0.1	0.15	0.13	0.29	0.36
160000	149.51	97.41	88.84	436.77	168.25	91.29	71.33	0.2	0.26	0.36	0.21	0.24	0.85	0.82
250000	274.3	131.46	151.32	841.76	306.77	139.76	121.73	0.35	0.40	0.6	0.41	0.52	1.25	1.26
1000000	1843	892.47	865.32	5951.45	1915.08	945.78	680.25	2.02	2.79	3.9	2.28	2.31	7.2	8.98
2250000	4929.21	1915.24	2273.57	-	5753.59	2351.16	1796.48	3.19	3.95	8.16	-	4.69	15.27	16.25
4000000	9241.3	3035.18	4342.54	-	11225.7	4615.09	3387.68	8.95	10.13	17.67	-	10.62	31.5	33.59
6250000	15890.4	4719.75	7322.53	-	18485.5	8086.97	5744.08	16.73	22.95	32.29	-	23.31	55.16	58.85

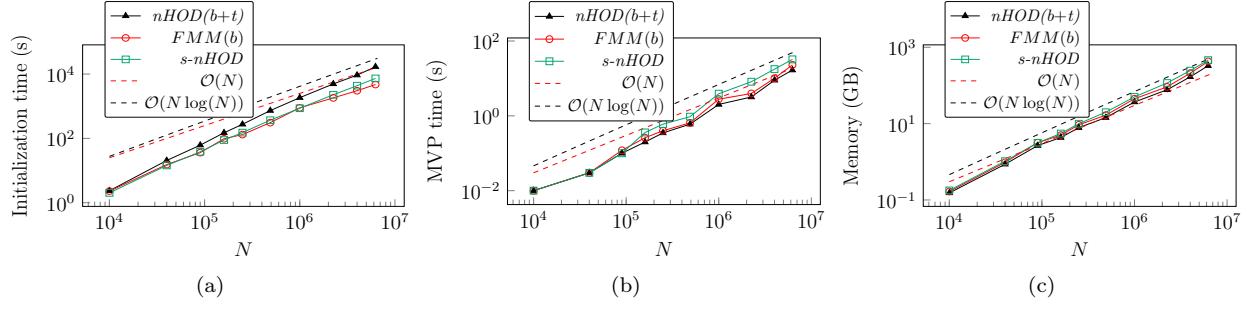
TABLE 11

Time comparison of the algorithms as mentioned in Table 7 for the kernel function $1/r$

N	Memory (GB)							Relative error in matrix-vector product (norm 2)						
	nHOD(b+t)	FMM(b)	s-nHOD	nHOD(t)	FMM(t)	HOD	\mathcal{H}	nHOD(b+t)	FMM(b)	s-nHOD	nHOD(t)	FMM(t)	HOD	\mathcal{H}
10000	0.1527	0.1666	0.1780	0.1524	0.1667	0.2393	0.2633	5.14E-12	3.75E-11	4.85E-11	8.69E-12	8.26E-13	9.74E-13	9.10E-14
40000	0.8613	0.9680	1.0408	0.9232	0.9764	1.4829	1.6762	1.85E-11	1.27E-10	1.95E-10	7.65E-12	2.82E-12	8.94E-13	1.27E-13
90000	2.6587	3.1650	3.1449	2.9132	3.1621	4.2674	4.9701	2.06E-11	7.67E-11	7.91E-11	2.52E-11	2.66E-12	1.85E-12	1.17E-13
160000	4.3113	5.0038	5.5146	4.8980	5.0110	8.2334	9.4448	2.10E-10	1.18E-10	2.06E-10	2.52E-11	3.69E-12	3.13E-12	1.25E-13
250000	7.8220	9.2904	9.9532	8.8927	9.3156	14.4371	16.6336	2.73E-10	1.23E-10	2.70E-10	2.01E-11	3.74E-12	2.50E-12	1.40E-13
1000000	36.766	44.8229	50.1022	42.5693	44.8932	75.2346	87.4024	3.57E-11	8.14E-11	3.53E-10	2.44E-11	6.44E-12	1.44E-11	1.10E-13
2250000	77.0181	91.6492	115.989	-	91.8749	186.878	214.366	8.46E-11	7.93E-12	1.55E-10	-	-	-	-
4000000	168.06	209.858	244.573	-	210.239	376.158	439.09	-	-	-	-	-	-	-
6250000	328.493	426.245	461.553	-	426.808	677.432	806.873	-	-	-	-	-	-	-

TABLE 12

Memory and relative error ($\epsilon = 10^{-12}$) of the algorithms as mentioned in Table 7 for the kernel function $1/r$

FIG. 10. Plots of initialization time (Figure 10a), MVP time (Figure 10b) and memory (Figure 10c) for $1/r$ **Experiment 3.**

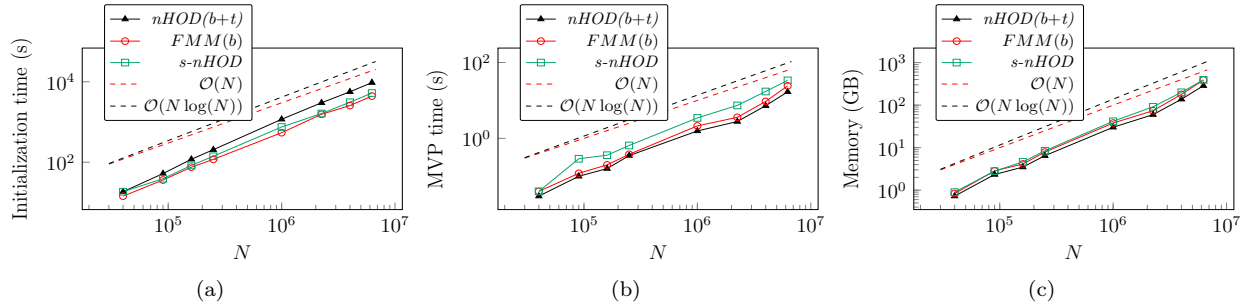
N	Initialization time (s)							MVP time (s)						
	$nHOD(b+t)$	$FMM(b)$	$s-nHOD$	$nHOD(t)$	$FMM(t)$	HOD	\mathcal{H}	$nHOD(b+t)$	$FMM(b)$	$s-nHOD$	$nHOD(t)$	$FMM(t)$	HOD	\mathcal{H}
40000	18.53	14.39	15.26	37.02	23.37	16.45	15.96	0.01	0.04	0.04	0.01	0.01	0.07	0.06
90000	52.23	36.17	38.99	113.85	62.1	43.05	41.87	0.12	0.12	0.29	0.13	0.13	0.21	0.27
160000	118.65	75.5	83.55	285.9	148.09	97.94	93.24	0.16	0.20	0.36	0.15	0.19	0.44	0.49
250000	205.06	117.93	141.06	496.35	255.71	168.87	158.65	0.35	0.38	0.65	0.36	0.42	1.23	1.34
1000000	1168.48	542.58	751.68	3465.28	1667.14	978.26	891.03	1.57	2.13	3.46	1.61	2.26	6.22	6.51
2250000	3007.37	1555.49	1626.07	12621.5	4211.65	1982.96	2077.81	2.78	3.59	7.39	3.3	3.86	11.89	13.81
4000000	5634.42	2559.35	3097.76	24333	8121.07	3941.29	4081.68	7.26	9.42	17.21	10.64	10.66	26.23	29.79
6250000	9522.67	4407.21	5242.37	43494.9	14880.4	6848.59	7153.45	16.87	24.2	33.79	18.28	28.57	51.46	55.85

TABLE 13

Time comparison of the algorithms as mentioned in Table 7 for the kernel function e^{-r}

N	Memory (GB)							Relative error in matrix-vector product (norm 2)						
	$nHOD(b+t)$	$FMM(b)$	$s-nHOD$	$nHOD(t)$	$FMM(t)$	HOD	\mathcal{H}	$nHOD(b+t)$	$FMM(b)$	$s-nHOD$	$nHOD(t)$	$FMM(t)$	HOD	\mathcal{H}
40000	0.7244	0.8330	0.9008	0.7783	0.8380	1.3040	1.5009	1.03E-12	1.40E-12	1.01E-12	8.30E-12	3.56E-12	5.91E-13	2.18E-13
90000	2.3320	2.8488	2.7984	2.4809	2.8562	3.8262	4.5858	1.86E-11	1.75E-11	1.85E-11	4.38E-10	2.31E-11	7.91E-12	4.64E-13
160000	3.4947	4.1328	4.6242	3.8982	4.1539	7.0722	8.3150	4.55E-10	3.82E-10	4.56E-10	7.69E-11	1.87E-11	1.48E-11	1.16E-12
250000	6.4726	7.8719	8.4406	7.1483	7.9119	12.5236	14.9071	2.85E-10	3.86E-10	2.71E-10	1.48E-10	1.28E-10	4.29E-12	6.32E-12
1000000	30.1564	37.9634	41.7328	33.4074	38.1141	63.9866	77.4723	4.94E-10	1.22E-10	1.30E-10	2.85E-10	2.42E-10	9.55E-11	4.21E-11
2250000	59.8536	73.968	91.4432	65.701	74.267	151.986	183.283	2.88E-10	8.66E-11	1.10E-10	-	-	-	-
4000000	137.644	178.976	200.472	151.42	179.621	314.004	385.474	-	-	-	-	-	-	-
6250000	286.551	389.097	392.889	304.242	389.904	576.213	724.665	-	-	-	-	-	-	-

TABLE 14

Memory and relative error ($\epsilon = 10^{-12}$) of the algorithms as mentioned in Table 7 for the kernel function e^{-r} FIG. 11. Plots of initialization time (Figure 11a), MVP time (Figure 11b) and memory (Figure 11c) for e^{-r} **Experiment 4.**

5.1.2. Fast iterative solver for a system arises from 2D Helmholtz kernel. In this experiment, we consider N uniformly distributed particles (source and target) at the location $\{\mathbf{x}_i\}_{i=1}^N$ over the domain

$[-1, 1]^2$. To have a well-conditioned system matrix, we set the $(i, j)^{th}$ entry as

$$(5.2) \quad K(i, j) = \begin{cases} \frac{i}{4} H_0^{(i)} (\|\mathbf{x}_i - \mathbf{x}_j\|_2) & \text{if } i \neq j \\ 250N & \text{otherwise} \end{cases}$$

We construct the following system by setting \mathbf{b} as in Table 8

$$(5.3) \quad K\boldsymbol{\lambda} = \mathbf{b}$$

We solve Equation (5.3) by the iterative solver GMRES and report the initialization time, solution time in Table 15 and memory in Table 16 for all the seven algorithms. The relative error in the solution is of order 10^{-12} in all the cases. We also plot the initialization time (Figure 12a), solution time (Figure 12b) and memory (Figure 12c) in Figure 12 to solve Equation (5.3).

N	Initialization time (s)							Solution time (s)						
	nHOD(b+t)	FMM(b)	s-nHOD	nHOD(t)	FMM(t)	HOD	\mathcal{H}	nHOD(b+t)	FMM(b)	s-nHOD	nHOD(t)	FMM(t)	HOD	\mathcal{H}
10000	4.58914	6.63167	6.23756	6.02415	12.442	9.45567	10.1272	0.05840	0.08328	0.09400	0.047305	0.55451	0.07170	0.08242
40000	21.2565	22.6638	36.4582	41.8131	245.03	60.6468	68.9379	0.17199	0.34505	0.22141	0.175771	0.82306	0.29615	0.34062
90000	60.5745	60.6287	84.539	114.863	399.06	148.733	169.298	0.38523	0.81794	0.79919	0.388909	1.00512	0.69657	0.77928
160000	139.539	151.289	199.742	279.55	1303.65	356.294	406.241	0.733328	1.5237	1.50714	0.746573	1.52415	1.51539	1.60616
250000	204.732	214.62	316.498	483.644	1468.36	568.279	653.346	1.35657	2.76504	3.50723	1.35375	2.45663	2.54275	2.59266
640000	752.232	2109.59	941.598	1689.16	3273.4	1869.72	2164.7	3.08859	5.62676	5.12754	3.24111	5.96424	6.90655	7.46378

TABLE 15
Time comparison of the algorithms as mentioned in Table 7 for the Equation (5.3)

N	Memory (GB)							#iter
	nHOD(b+t)	FMM(b)	s-nHOD	nHOD(t)	FMM(t)	HOD	\mathcal{H}	
10000	0.0900041	0.119028	0.107454	0.0910004	0.11869	0.144523	0.144764	4
40000	0.403489	0.546446	0.53134	0.423301	0.546548	0.803703	0.873257	4
90000	1.494	2.28461	1.81444	1.50942	2.2832	2.47536	2.59579	4
160000	1.71618	2.34106	2.55115	1.83665	2.33773	4.24159	4.78254	4
250000	3.37126	4.94592	4.68807	3.53943	4.94172	7.40971	8.26048	4
640000	7.09085	9.70095	11.8185	7.72916	9.66627	20.9687	24.3254	4

TABLE 16
Memory comparison of the algorithms as mentioned in Table 7 for the Equation (5.3)

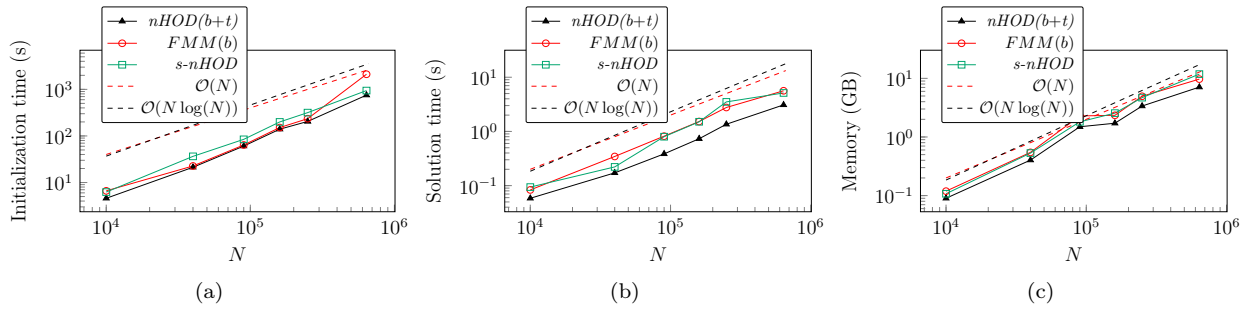


FIG. 12. Various benchmarks of the algorithms nHOD(b+t), FMM(b) and s-nHOD for the Equation (5.3)

Experiment 5.

5.1.3. Fast matrix-vector product accelerated GMRES for RBF interpolation in 2D. We consider N uniformly distributed particles at the location $\{\mathbf{x}_i\}_{i=1}^N$ over the domain $[-1, 1]^2$ and the kernel function $F : \mathbb{R} \rightarrow \mathbb{R}$ is given by

$$(5.4) \quad F(r) = \begin{cases} a/r & \text{if } r \geq a \\ r/a & \text{if } r < a \end{cases}$$

Consider the linear system (Equation (5.5)) generated by the kernel function F

$$(5.5) \quad \alpha \lambda_i + \sum_{j=1, j \neq i}^N F(\|\mathbf{x}_i - \mathbf{x}_j\|_2) \lambda_j = b_i$$

We set $a = 0.0001$ and $\alpha = 1$. By setting \mathbf{b} as in Table 8, the linear system Equation (5.5) can be written in the form

$$(5.6) \quad K\lambda = \mathbf{b}$$

We solve Equation (5.6) using GMRES and report the initialization time, solution time in Table 17, memory and relative error in the solution in Table 18 for all the seven algorithms. We also plot the initialization time (Figure 13a), solution time (Figure 13b) and memory (Figure 13c) in Figure 13 to solve the Equation (5.6).

N	Initialization time (s)							Solution time (s)						
	$nHOD(b+t)$	$FMM(b)$	$s-nHOD$	$nHOD(t)$	$FMM(t)$	HOD	\mathcal{H}	$nHOD(b+t)$	$FMM(b)$	$s-nHOD$	$nHOD(t)$	$FMM(t)$	HOD	\mathcal{H}
10000	3.68107	3.31348	4.1444	6.0666	3.66517	2.16876	1.75493	0.12545	0.15902	0.130214	0.12099	0.117634	0.10868	0.18249
40000	29.635	25.4584	18.7056	67.5184	31.5676	15.2949	12.3136	0.85386	0.81117	1.02531	0.995413	0.819762	0.872288	1.13964
90000	82.5265	59.0323	43.8586	221.309	82.0278	37.7838	26.2808	2.10774	2.66373	2.88704	2.38313	2.6997	2.74979	3.44596
160000	210.103	153.429	110.125	532.642	227.152	95.9747	72.954	6.26587	6.2993	6.34722	7.53588	6.61342	7.56773	9.72869
250000	375.288	225.979	171.604	991.591	382.123	156.892	114.086	10.2358	10.3649	12.9162	12.3281	10.21156	14.1423	17.2826
490000	989.93	599.425	448.191	2735.43	1021.14	436.045	322.771	34.2433	35.0495	45.7259	41.4253	36.5963	47.6453	59.0032
1000000	2462.17	1086.07	890.46	7040.31	2599.98	901.409	702.476	82.9376	92.7408	110.538	94.8872	85.162	121.292	155.541
1210000	2788.3	1248.61	1106.24	9031.52	3248.88	-	-	95.317	109.429	184.01	100.932	98.8271	-	-
2250000	6098.63	2786.67	2687.35	-	7664.26	-	-	231.614	383.745	416.71	-	413.203	-	-

TABLE 17
Time comparison of the algorithms as mentioned in Table 7 for the Equation (5.6)

N	Memory (GB)							Relative error in solution (norm 2)							#iter
	$nHOD(b+t)$	$FMM(b)$	$s-nHOD$	$nHOD(t)$	$FMM(t)$	HOD	\mathcal{H}	$nHOD(b+t)$	$FMM(b)$	$s-nHOD$	$nHOD(t)$	$FMM(t)$	HOD	\mathcal{H}	
10000	0.19388	0.21446	0.21069	0.21693	0.21467	0.25921	0.250362	1.14E-12	1.01E-12	1.10E-12	8.05E-13	7.70E-13	7.69E-13	7.59E-13	12
40000	1.0013	1.14909	1.16588	1.20412	1.14782	1.56176	1.61375	1.10E-12	6.81E-12	1.08E-12	2.84E-12	5.50E-13	3.88E-13	1.78E-13	20
90000	2.47351	3.04545	3.03009	2.96977	3.05347	4.18	4.14545	6.63E-12	1.10E-11	5.46E-12	4.27E-12	8.36E-13	7.66E-13	5.76E-13	27
160000	4.60248	5.34647	5.89149	5.78094	5.35437	8.52	9.06706	2.18E-12	5.18E-12	6.73E-12	8.09E-12	7.25E-13	7.53E-13	3.68E-13	34
250000	7.08151	8.32165	9.4008	9.01161	8.34077	14.08	14.7513	2.40E-11	2.13E-11	2.03E-11	1.42E-11	1.29E-12	4.81E-12	6.15E-13	41
490000	15.7234	18.1537	21.4673	19.7996	18.3524	32.4142	35.7932	5.29E-11	1.82E-11	4.70E-11	2.89E-11	1.90E-12	2.96E-12	5.11E-13	54
1000000	30.0574	35.2533	44.8842	39.2645	35.298	71.41	75.9143	3.39E-11	1.01E-11	1.85E-11	3.02E-11	2.05E-12	8.34E-12	5.22E-13	73
1210000	37.0432	44.1436	56.2672	48.3545	44.133	-	-	4.65E-11	1.45E-11	2.91E-11	3.75E-11	2.61E-12	-	-	79
2250000	73.7261	85.5905	114.506	-	84.336	-	-	8.01E-11	3.22E-11	6.69E-11	-	4.54E-12	-	-	104

TABLE 18
Memory and relative error in the solution of the algorithms as mentioned in Table 7 for the Equation (5.6)

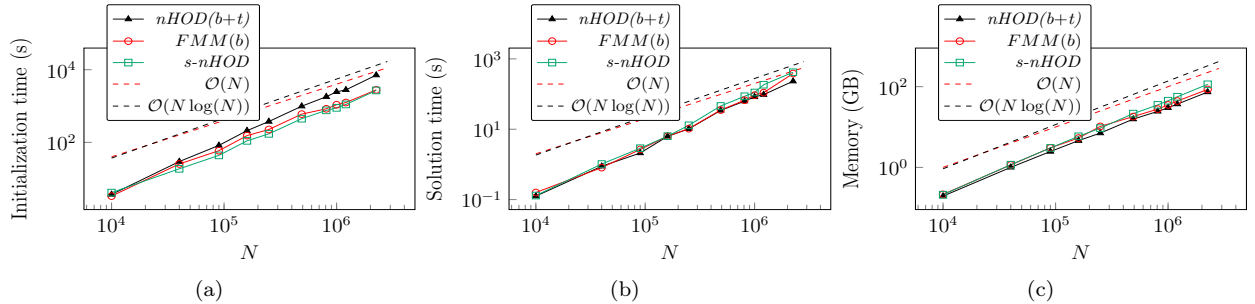


FIG. 13. Various benchmarks of the algorithms $nHOD(b+t)$, $FMM(b)$ and $s-nHOD$ for the Equation (5.6)

Experiment 6.

5.1.4. Fast matrix-vector product accelerated GMRES for integral equation in 2D. In this experiment, we consider the Fredholm integral equation of the second kind over $C = [-1, 1]^2 \subset \mathbb{R}^2$, which is

given by

$$(5.7) \quad \sigma(\mathbf{x}) + \int_C F(\mathbf{x}, \mathbf{y}) \sigma(\mathbf{y}) d\mathbf{y} = f(\mathbf{x}) \quad \mathbf{x}, \mathbf{y} \in C$$

with $F(\mathbf{x}, \mathbf{y}) = -\frac{1}{2\pi} \log(\|\mathbf{x} - \mathbf{y}\|_2)$ (Green's function for Laplace equation in 2D). We follow a piece-wise constant collocation method with collocation points on a uniform grid in $C = [-1, 1]^2$ with weights $1/N$ to discretize (5.7) and set the RHS \mathbf{f} as described in Table 8. Therefore, we obtain the following linear system

$$(5.8) \quad K\sigma = \mathbf{f}$$

We solve Equation (5.8) using GMRES and report the initialization time, solution time in Table 19 and memory, relative error in Table 20 for all the seven algorithms. We also plot the initialization time (Figure 14a), solution time (Figure 14b) and memory (Figure 14c) in Figure 14 to solve Equation (5.8).

N	Initialization time (s)							Solution time (s)						
	nHOD(b+t)	FMM(b)	s-nHOD	nHOD(t)	FMM(t)	HOD	\mathcal{H}	nHOD(b+t)	FMM(b)	s-nHOD	nHOD(t)	FMM(t)	HOD	\mathcal{H}
10000	0.9327	0.7013	1.02954	1.352	1.0091	1.20583	1.26959	0.0327	0.0364	0.0385	0.0363	0.0564	0.0667	0.0676
40000	6.1622	3.8255	9.8493	11.0285	9.2599	7.92065	8.73945	0.1302	0.1613	0.1706	0.1297	0.2054	0.3084	0.2607
90000	15.7789	8.8914	18.555	33.4066	25.0651	18.4323	19.6975	0.2850	0.3726	0.3874	0.2805	0.5653	0.6649	0.6045
160000	36.4931	18.9178	39.8861	84.3524	65.8172	45.6604	51.8981	0.5510	0.7103	0.8121	0.5667	0.9757	1.2659	1.3398
250000	61.3042	28.0676	64.9068	155.197	110.013	71.4705	80.4164	0.7551	1.0141	1.2198	0.7553	1.4689	1.7661	1.6749
490000	166.493	65.092	165.191	405.848	296.36	185.253	217.612	1.9172	2.3499	2.9002	1.8327	3.2487	5.0667	4.8941
1000000	334.728	126.183	330.17	985.319	665.706	390.853	460.025	2.6406	3.7614	5.1719	2.7779	5.3191	7.9763	8.5925
1210000	420.135	154.349	410.548	1273.98	821.33	480.659	563.637	3.8892	5.1248	7.1155	3.8770	7.0558	11.63	11.9131
1440000	514.494	182.349	543.678	1593.64	999.4	592.696	-	4.5442	6.6623	8.5384	5.0893	8.2723	14.731	-

TABLE 19

Time comparison of the algorithms as mentioned in Table 7 for the Equation (5.8)

N	Memory (GB)							Relative error in solution (norm 2)							#iter
	nHOD(b+t)	FMM(b)	s-nHOD	nHOD(t)	FMM(t)	HOD	\mathcal{H}	nHOD(b+t)	FMM(b)	s-nHOD	nHOD(t)	FMM(t)	HOD	\mathcal{H}	
10000	0.0905	0.1199	0.1083	0.0927	0.1197	0.1459	0.146351	3.46E-13	3.30E-13	3.31E-13	3.32E-13	3.32E-13	3.30E-13	3.30E-13	6
40000	0.4076	0.5512	0.5415	0.4269	0.5503	0.8214	0.888925	2.13E-13	1.43E-13	1.49E-13	2.14E-13	1.48E-13	1.47E-13	1.48E-13	6
90000	1.4998	2.28454	1.8413	1.5235	2.2826	2.52	2.62389	3.62E-13	6.48E-14	6.63E-14	3.32E-13	6.49E-14	6.54E-14	6.49E-14	6
160000	1.7245	2.3657	2.566	1.8554	2.3619	4.27	4.84742	4.66E-13	2.52E-13	2.53E-14	2.91E-13	2.66E-14	2.61E-14	2.63E-14	6
250000	3.39	4.94135	4.751	3.5739	4.9321	7.50	8.33867	6.03E-13	7.60E-14	7.97E-14	2.27E-13	7.56E-14	7.85E-14	7.56E-14	6
490000	5.0355	6.5684	8.5181	7.7417	6.5513	15.4568	18.2648	2.61E-13	6.46E-14	6.78E-14	2.77E-13	6.44E-14	6.40E-14	6.41E-14	6
1000000	13.8422	20.2473	21.6591	14.6255	20.2237	36.5053	41.6402	5.28E-13	7.86E-13	7.87E-13	8.91E-13	7.81E-13	7.81E-13	7.81E-13	5
1210000	18.7613	28.4799	28.5305	19.5536	28.4477	46.6362	52.6718	5.26E-13	4.39E-14	5.70E-14	8.94E-13	4.31E-14	6.00E-14	4.30E-14	6
1440000	25.2567	39.2602	37.1569	26.029	39.2231	58.8965	-	3.88E-13	3.04E-13	2.85E-14	7.97E-13	2.96E-14	2.99E-14	-	6

TABLE 20

Memory and relative error in the solution of the algorithms as mentioned in Table 7 for the Equation (5.8)

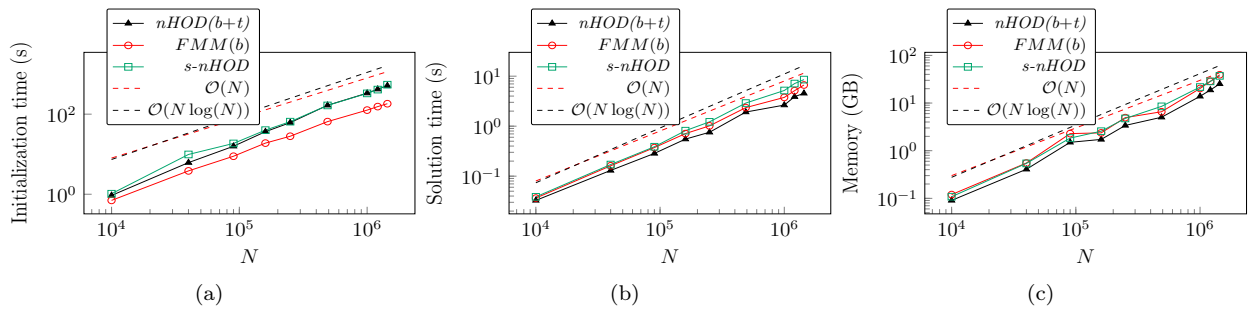


FIG. 14. Various benchmarks of the algorithms $nHOD(b+t)$, $FMM(b)$ and $s-nHOD$ for the Equation (5.8)

Remark 5.3. It is to be noted that the initialization time of the proposed $nHOD(b+t)$ performs way better than the $nHOD(t)$ algorithm. The initialization cost of the $nHOD(t)$ algorithm is the highest.

Remark 5.4. In all the experiments in 2D, the proposed $nHOD(b+t)$ beats all the other algorithms in terms of matrix-vector product time and memory. If we consider the initialization time as a one-time cost, then $nHOD(b+t)$ could be useful for the 2D problems where the number of iterations is large in the iterative method.

5.2. Experiments in three dimensions. In this subsection, we perform various experiments in 3D. We consider N overlapping source and target points for all the experiments.

5.2.1. Fast matrix-vector product in 3D. Below, we report the results for four different kernel functions on the different distributions of the particles.

1. $F(r) = 1/r$ (single layer Laplacian in 3D) Table 21, Table 22 and Figure 15
2. $F(r) = 1/r^4$ Table 23, Table 24 and Figure 16
3. $F(r) = e^{ir}/r$ (Helmholtz kernel with wavenumber = 1 in 3D) Table 25, Table 26 and Figure 17
4. $F(r) = \frac{1}{8\pi} \left(\frac{1}{r} I + \frac{r \otimes r}{r^3} \right)$ (single layer Stokes kernel in 3D) Table 27, Table 28 and Figure 18

We consider the N overlapping source and target as the $N^{1/3} \times N^{1/3} \times N^{1/3}$ tensor product grid on Chebyshev nodes in the cube $[-1, 1]^3$ for the first three kernel functions ($1/r$, $1/r^4$ and Helmholtz kernel), and N random uniformly distributed overlapping source and target in $[-1, 1]^3$ for the last kernel function (Stokes kernel). We take 5 different column vectors ϕ and tabulate the average initialization time, MVP time, memory and relative error of all the seven fast matrix-vector algorithms (as mentioned in Table 7) in Tables 21 to 28. In Figures 15 to 18, we plot the scaling of the initialization time, average MVP time and memory for the algorithms $nHOD(b+t)$, $FMM(b)$ and $s-nHOD$ (as mentioned in Table 7).

Experiment 7.

N	Initialization time (s)							MVP time (s)						
	$nHOD(b+t)$	$FMM(b)$	$s-nHOD$	$nHOD(t)$	$FMM(t)$	HOD	\mathcal{H}	$nHOD(b+t)$	$FMM(b)$	$s-nHOD$	$nHOD(t)$	$FMM(t)$	HOD	\mathcal{H}
27000	27.03	36.2	26.34	21.78	23.37	8.05	7.14	0.04	0.05	0.04	0.05	0.05	0.07	0.09
64000	85.96	120.55	80.66	130.55	118.27	41.91	39.76	0.12	0.13	0.13	0.12	0.19	0.29	0.43
125000	221.28	308.25	205.86	391.34	347.06	95.3	89.13	0.32	0.43	0.34	0.35	0.43	0.69	0.87
216000	533.49	739.45	488.62	893.52	749.13	184.33	169.62	0.75	1.25	0.99	0.86	0.85	1.86	1.66
512000	1754.3	2434.62	1557.58	3889.89	3072.75	757.44	718.81	1.78	2.39	2.3	1.8	1.82	6.82	6.99
729000	2790.13	3795.26	2432.97	6363.05	4937.31	1170.16	1127.4	2.96	4.2	3.71	3.03	3.87	10.12	10.24
1000000	4228.35	5720.23	3629.59	10114.4	7512.7	1686.4	1702.65	4.01	6.67	5.8	4.18	5.76	13.08	15.37
2197000	12646.3	13407.5	12198.5	32975.4	23721.7	5248.78	5533.09	9.01	12.3	12.5	9.13	12.2	40.43	42.82

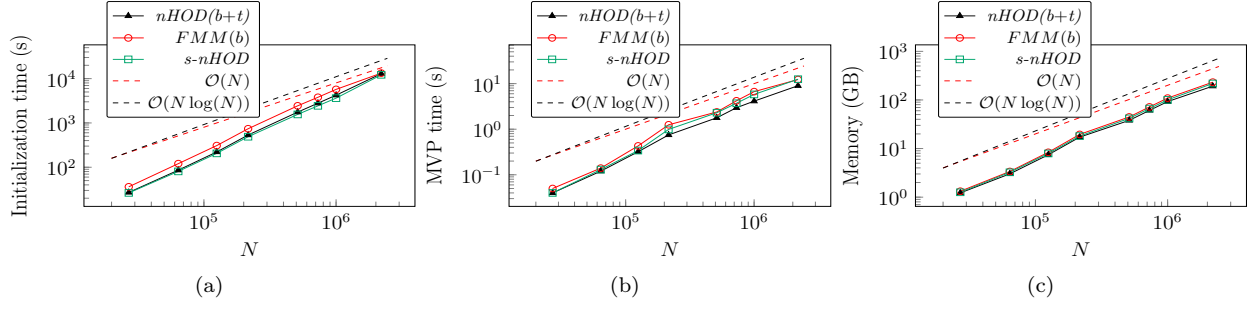
TABLE 21

Time comparison of the algorithms as mentioned in Table 7 for the kernel function $1/r$

N	Memory (GB)							Relative error in matrix-vector product (norm 2)						
	$nHOD(b+t)$	$FMM(b)$	$s-nHOD$	$nHOD(t)$	$FMM(t)$	HOD	\mathcal{H}	$nHOD(b+t)$	$FMM(b)$	$s-nHOD$	$nHOD(t)$	$FMM(t)$	HOD	\mathcal{H}
27000	1.2223	1.3244	1.26005	1.23366	1.32443	1.67239	1.79788	2.12E-07	2.86E-07	1.88E-07	3.02E-07	2.86E-07	5.40E-08	3.53E-08
64000	3.0150	3.3765	3.24437	3.15943	3.36643	5.69102	6.23738	8.82E-07	9.50E-07	6.89E-07	1.42E-06	5.06E-07	1.00E-07	7.53E-08
125000	7.4363	8.3697	7.92428	7.93908	8.40858	13.2553	14.4525	1.72E-06	8.01E-07	1.41E-06	1.27E-06	6.64E-07	1.58E-07	1.13E-07
216000	17.1614	19.5372	18.0705	17.9133	19.4772	27.3749	30.0646	1.51E-06	1.01E-06	1.15E-06	2.07E-06	9.96E-07	1.45E-07	1.13E-07
512000	37.9782	44.6665	41.7738	42.1566	44.5848	79.5325	88.7651	2.20E-06	2.32E-06	1.23E-06	3.60E-06	1.37E-06	2.50E-07	1.55E-07
729000	60.9414	71.9025	66.4761	68.1249	71.8001	121.506	136.058	3.37E-06	1.39E-06	1.95E-06	5.85E-06	1.19E-06	2.95E-07	1.35E-07
1000000	92.4869	109.151	100.467	103.743	108.659	178.994	200.22	4.39E-06	1.37E-06	2.02E-06	5.99E-06	1.55E-06	7.57E-07	1.71E-07
2197000	192.349	232.337	218.178	220.488	231.302	469.946	534.111	4.69E-06	1.84E-06	2.79E-06	6.98E-06	2.65E-06	7.60E-06	2.89E-07

TABLE 22

Memory and relative error ($\epsilon = 10^{-7}$) of the algorithms as mentioned in Table 7 for the kernel function $1/r$

FIG. 15. Plots of initialization time (Figure 15a), MVP time (Figure 15b) and memory (Figure 15c) for $1/r$ **Experiment 8.**

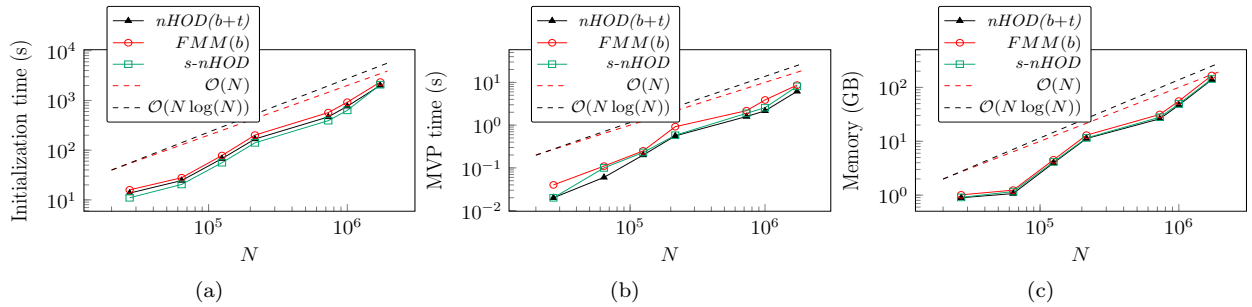
N	Initialization time (s)							MVP time (s)						
	$nHOD(b+t)$	$FMM(b)$	$s-nHOD$	$nHOD(t)$	$FMM(t)$	HOD	\mathcal{H}	$nHOD(b+t)$	$FMM(b)$	$s-nHOD$	$nHOD(t)$	$FMM(t)$	HOD	\mathcal{H}
27000	13.68	15.89	11.02	13.5	15.27	19.25	21.49	0.02	0.04	0.02	0.04	0.05	0.07	0.04
64000	24.5	27.91	20.43	29.49	34.12	63.96	75.13	0.06	0.11	0.1	0.09	0.09	0.17	0.19
125000	67.63	78.06	56.05	80.05	91.84	144.05	168.83	0.2	0.25	0.23	0.24	0.26	0.44	0.54
216000	167.61	201.04	140.44	189.41	221.05	302.04	354.21	0.56	0.92	0.58	0.74	0.93	1.1	1.15
729000	466.54	569.53	392.07	657.05	768.46	1345.5	1633.31	1.59	2.18	1.89	1.6	2.11	4.02	4.87
1000000	664.1	921.56	633.1	1038.2	1244.05	1981.84	2413.35	2.16	3.88	2.56	3.31	3.59	5.79	7.63
1728000	2008.73	2344.53	2076.88	2560.08	2894.28	4502.09	5012.17	6.17	8.64	8.58	8.11	9.55	20.35	21.25

TABLE 23

Time comparison of the algorithms as mentioned in Table 7 for the kernel function $1/r^4$

N	Memory (GB)							Relative error in matrix-vector product (norm 2)						
	$nHOD(b+t)$	$FMM(b)$	$s-nHOD$	$nHOD(t)$	$FMM(t)$	HOD	\mathcal{H}	$nHOD(b+t)$	$FMM(b)$	$s-nHOD$	$nHOD(t)$	$FMM(t)$	HOD	\mathcal{H}
27000	0.88696	1.01237	0.90881	0.893662	1.01237	1.18831	1.34361	1.98E-13	6.74E-14	7.76E-14	2.18E-13	7.30E-14	1.40E-09	1.41E-08
64000	1.04345	1.23792	1.16398	1.06962	1.22868	2.9189	3.429	5.67E-13	3.23E-06	3.36E-08	5.24E-05	5.32E-05	2.55E-05	2.55E-04
125000	3.91642	4.52006	4.12692	3.95483	4.51326	7.44811	8.63971	6.40E-13	3.86E-06	2.20E-09	2.95E-05	2.23E-05	2.01E-07	2.53E-06
216000	11.1665	12.9778	11.5302	11.2272	12.9657	17.2641	20.1067	1.28E-12	1.09E-06	2.45E-13	2.82E-05	4.31E-03	1.36E-06	1.37E-05
729000	25.8388	31.444	27.9152	26.084	31.3394	62.1285	75.4767	8.47E-08	4.32E-05	6.14E-09	9.38E-05	8.85E-05	2.01E-07	2.53E-06
1000000	46.5	55.6658	49.3195	46.8175	55.5638	96.2987	116.188	3.41E-07	4.38E-05	2.25E-09	4.26E-05	6.95E-04	4.49E-05	4.49E-04
1728000	138.463	166.622	143.219	138.939	166.456	223.461	269.84	-	-	-	-	-	-	-

TABLE 24

Memory and relative error ($\epsilon = 10^{-7}$) of the algorithms as mentioned in Table 7 for the kernel function $1/r^4$ FIG. 16. Plots of initialization time (Figure 16a), MVP time (Figure 16b) and memory (Figure 16c) for $1/r^4$ **Experiment 9.**

N	Initialization time (s)							MVP time (s)						
	$nHOD(b+t)$	$FMM(b)$	$s-nHOD$	$nHOD(t)$	$FMM(t)$	HOD	\mathcal{H}	$nHOD(b+t)$	$FMM(b)$	$s-nHOD$	$nHOD(t)$	$FMM(t)$	HOD	\mathcal{H}
27000	72.17	76.79	68.95	78.33	91.56	36.39	36.84	0.17	0.26	0.24	0.17	0.26	0.33	0.34
64000	235.62	246.78	221.75	403.55	415.72	154.99	165.85	0.45	0.64	0.55	0.59	0.68	1.39	1.37
125000	588.51	619.98	544.94	1175.71	1123.51	348.58	364.67	1.52	1.58	1.47	1.55	1.86	2.73	3.29
216000	1371.53	1447.1	1253.82	2619.92	2446.55	671.65	693.85	2.86	3.44	2.96	3.16	4.15	6.88	7.07
512000	4319.89	4557.4	3838.07	10835.9	9644.96	2359.52	2500.58	6.3	7.5	7.03	7.15	8.38	20.44	22.74
729000	6938.2	7142.6	5957.71	17891.5	15062.4	3583.2	3744.72	10.71	13.18	12.91	12.38	14.22	33.67	33.81
1000000	10073.4	10984	8839.64	29905.1	22480.2	5320.56	5461.07	16.31	20.39	19.47	19.21	21.95	47.87	48.66

TABLE 25

Time comparison of the algorithms as mentioned in Table 7 for the kernel function $e^{i\mathbf{r}}/r$ (Helmholtz kernel in 3D)

N	Memory (GB)							Relative error in matrix-vector product (norm 2)						
	$nHOD(b+t)$	$FMM(b)$	$s-nHOD$	$nHOD(t)$	$FMM(t)$	HOD	\mathcal{H}	$nHOD(b+t)$	$FMM(b)$	$s-nHOD$	$nHOD(t)$	$FMM(t)$	HOD	\mathcal{H}
27000	1.20864	1.30981	1.25037	1.22964	1.30981	1.68292	1.8075	3.97E-07	3.75E-07	3.33E-07	4.63E-07	3.75E-07	6.16E-08	4.53E-08
64000	2.9802	3.36391	3.21018	3.15951	3.34046	5.72371	6.28585	1.25E-06	8.46E-07	1.02E-06	1.15E-06	7.83E-07	2.55E-07	8.74E-08
125000	7.4571	8.3484	7.9395	7.9431	8.34997	13.2916	14.5086	1.81E-06	1.91E-06	1.67E-06	2.34E-06	8.48E-07	2.23E-07	1.25E-07
216000	17.1152	19.3999	18.0723	17.9491	19.4075	27.4697	30.156	1.49E-06	1.14E-06	1.16E-06	1.94E-06	1.10E-06	1.70E-07	1.28E-07
512000	37.9649	44.5358	41.6825	42.019	44.5309	79.6991	89.1343	2.22E-06	1.87E-06	1.81E-06	3.29E-06	1.26E-06	2.99E-07	1.70E-07
729000	60.9265	71.7619	66.4551	67.9485	71.5148	121.861	136.598	3.36E-06	2.01E-06	2.42E-06	5.77E-06	1.74E-06	1.06E-06	1.29E-07
1000000	92.5229	108.913	100.594	103.699	108.398	179.47	200.838	3.52E-06	2.29E-06	2.05E-06	5.29E-06	1.95E-06	2.26E-07	9.71E-08

TABLE 26

Memory and relative error ($\epsilon = 10^{-7}$) of the algorithms as mentioned in Table 7 for the kernel function $e^{i\mathbf{r}}/r$

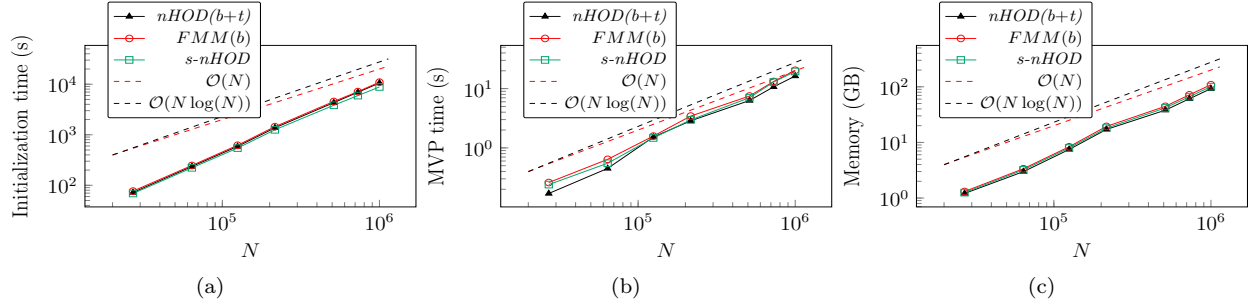


FIG. 17. Plots of initialization time (Figure 17a), MVP time (Figure 17b) and memory (Figure 17c) for $e^{i\mathbf{r}}/r$

Experiment 10.

N	Initialization time (s)							MVP time (s)						
	$nHOD(b+t)$	$FMM(b)$	$s-nHOD$	$nHOD(t)$	$FMM(t)$	HOD	\mathcal{H}	$nHOD(b+t)$	$FMM(b)$	$s-nHOD$	$nHOD(t)$	$FMM(t)$	HOD	\mathcal{H}
8000	39.85	40.11	40.46	41.57	43.8	37.19	38.41	0.01	0.01	0.02	0.01	0.02	0.03	0.03
27000	147.94	150.93	164.69	173.95	183.89	135.65	142.65	0.11	0.15	0.11	0.12	0.14	0.15	0.2
64000	820.35	821.49	844	1037.24	1081.9	712.3	757.84	0.24	0.39	0.27	0.24	0.45	0.77	0.88
125000	3460.63	3834.06	3529	4757.3	4779.98	2197.19	2347.88	0.92	1.47	1.24	1.12	2.01	2.18	2.2
216000	5211.41	5726.82	5310.47	7622.44	8215.23	3669.38	4048.49	1.54	2.38	2.09	1.6	3.11	4.16	4.28

TABLE 27

Time comparison of the algorithms as mentioned in Table 7 for the Stokes kernel in 3D

N	Memory (GB)							Relative error in matrix-vector product (norm 2)						
	$nHOD(b+t)$	$FMM(b)$	$s-nHOD$	$nHOD(t)$	$FMM(t)$	HOD	\mathcal{H}	$nHOD(b+t)$	$FMM(b)$	$s-nHOD$	$nHOD(t)$	$FMM(t)$	HOD	\mathcal{H}
8000	0.43774	0.462196	0.453354	0.435611	0.462196	0.605792	0.630719	2.74E-05	2.70E-05	2.74E-05	2.87E-05	2.70E-05	4.60E-05	4.60E-05
27000	1.54307	1.66918	1.59052	1.617	1.66918	2.12897	2.26736	1.69E-07	1.82E-07	1.61E-07	1.96E-07	1.82E-07	4.57E-08	4.22E-08
64000	6.11915	6.74526	6.43706	6.55354	6.73329	9.77503	10.5711	1.37E-06	1.54E-06	1.33E-06	1.17E-06	1.10E-06	2.07E-07	1.95E-07
125000	21.6566	25.6319	22.7694	24.322	25.6366	28.4239	31.3946	1.75E-06	1.62E-06	1.67E-06	1.62E-06	1.54E-06	2.45E-07	2.25E-07
216000	32.3054	39.1869	34.4475	36.4205	39.17570	48.446	55.1771	7.85E-07	6.80E-07	6.28E-07	9.09E-07	6.47E-07	1.71E-07	1.34E-07

TABLE 28

Memory and relative error ($\epsilon = 10^{-7}$) of the algorithms as mentioned in Table 7 for the Stokes kernel in 3D

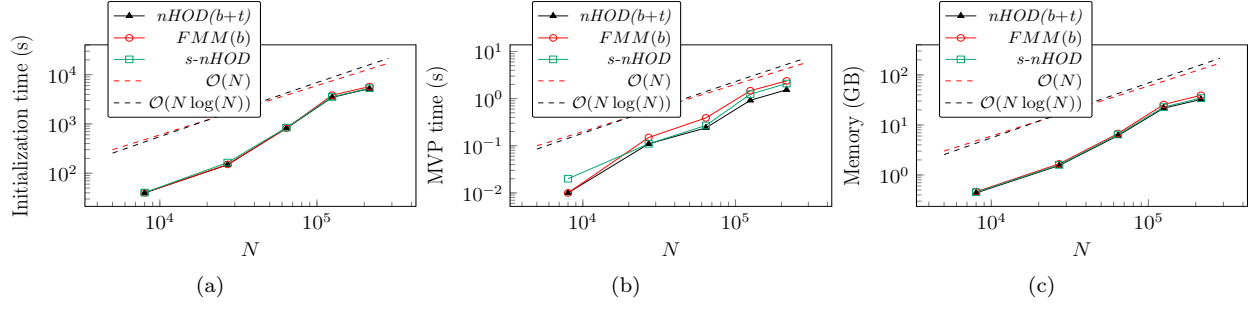


FIG. 18. Plots of initialization time (Figure 18a), MVP time (Figure 18b) and memory (Figure 18c) for Stokes kernel

The term $r \otimes r$ is the most expensive part of generating the matrix entries. That is why the initialization cost is very high for the Stokes kernel, even for a small value of N .

Experiment 11.

5.2.2. Fast iterative solver for a system arises from 3D Helmholtz kernel. In this experiment, we consider N uniformly distributed particles (source and target) at the location $\{\mathbf{x}_i\}_{i=1}^N$ in the domain $[-1, 1]^3$. To have a well-conditioned kernel matrix, we set the $(i, j)^{th}$ entry as

$$(5.9) \quad K(i, j) = \begin{cases} \frac{1}{4\pi} \frac{e^{ir}}{r} & \text{if } i \neq j \\ 500\sqrt{N} & \text{otherwise} \end{cases}$$

We construct following the system by setting \mathbf{b} as in Table 8

$$(5.10) \quad K\lambda = \mathbf{b}$$

We solve Equation (5.10) by the iterative solver GMRES and report the initialization time, solution time in Table 29 and memory in Table 30 for all the seven algorithms. The relative error in the solution is of order 10^{-7} in all the cases. We also plot the initialization time (Figure 19a), solution time (Figure 19b) and memory (Figure 19c) in Figure 19 to solve Equation (5.10).

N	Initialization time (s)							Solution time (s)						
	nHOD(b+t)	FMM(b)	s-nHOD	nHOD(t)	FMM(t)	HOD	\mathcal{H}	nHOD(b+t)	FMM(b)	s-nHOD	nHOD(t)	FMM(t)	HOD	\mathcal{H}
27000	41.6433	52.8429	43.7235	102.375	47.7773	30.6974	27.0977	0.5046	0.60407	0.556197	0.754304	0.578569	1.01984	0.899206
64000	301.48	358.185	281.116	593.678	366.013	176.405	181.258	3.48496	4.3571	3.50952	6.56525	4.16662	5.48467	6.58565
125000	716.523	752.491	619.679	1606.41	890.322	360.069	351.87	4.74324	5.85695	5.9331	7.13124	5.58666	9.91933	10.1532
216000	1234.94	1297.97	1057.38	3096.5	1598.8	644.847	613.493	6.40456	8.34409	7.49188	9.24278	7.92444	18.1242	19.1046
343000	2988.48	3403.62	2600.84	6903.14	3935.33	-	-	20.4612	27.5629	23.876	35.3912	32.1492	-	-
512000	4864.05	-	4191.69	12611.3	-	-	-	44.5926	-	55.9121	82.671	-	-	-
729000	7023.13	-	6082.16	-	-	-	-	65.0099	-	85.646	-	-	-	-

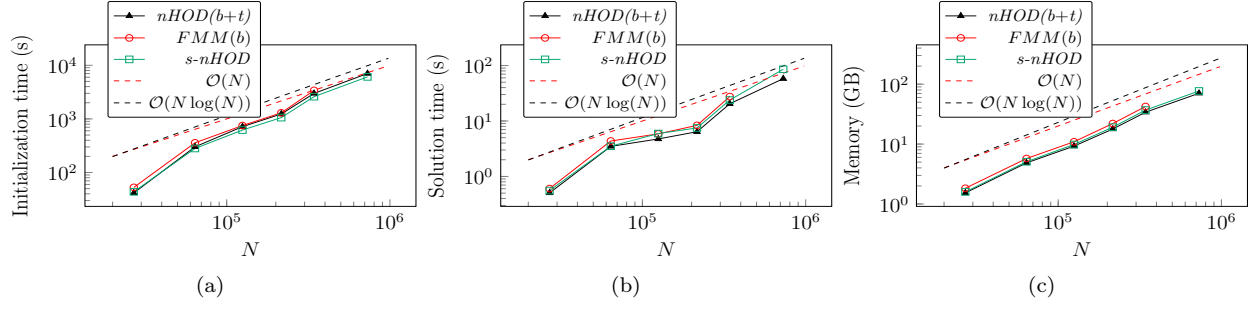
TABLE 29

Time comparison of the algorithms as mentioned in Table 7 for the Equation (5.10)

N	Memory (GB)							#iter
	nHOD(b+t)	FMM(b)	s-nHOD	nHOD(t)	FMM(t)	HOD	\mathcal{H}	
27000	1.52882	1.82916	1.58934	1.65773	1.82916	2.06412	2.36824	6
64000	4.84675	5.73455	5.07103	5.96492	5.77223	6.79439	7.61209	6
125000	9.23166	10.9167	9.8269	11.7847	11.0633	14.9248	17.0837	6
216000	17.8227	22.0168	19.1039	21.5594	22.1002	30.2939	35.6205	6
343000	34.0082	42.3677	36.9067	40.9892	42.423	-	-	6
512000	52.4457	-	56.6202	68.7857	-	-	-	7
729000	70.4469	-	76.8923	-	-	-	-	7

TABLE 30

Memory comparison of the algorithms as mentioned in Table 7 for the Equation (5.10)

FIG. 19. Various benchmarks of the algorithms $nHOD(b+t)$, $FMM(b)$ and $s-nHOD$ for the Equation (5.10)**Experiment 12.**

5.2.3. Fast matrix-vector product accelerated GMRES for RBF interpolation in 3D. We consider N uniformly distributed particles at the location $\{\mathbf{x}_i\}_{i=1}^N$ in the domain $[-1, 1]^3$ and the kernel function $F : \mathbb{R} \rightarrow \mathbb{R}$ is given by

$$(5.11) \quad F(r) = \begin{cases} \log r & \text{if } r \geq a \\ \frac{\log a}{r \log r - 1} & \text{if } r < a \end{cases}$$

Consider the linear system (Equation (5.12)) generated by the above kernel function F

$$(5.12) \quad \alpha \lambda_i + \sum_{j=1, j \neq i}^N F(\|\mathbf{x}_i - \mathbf{x}_j\|_2) \lambda_j = b_i$$

We set $a = 0.0001$ and $\alpha = \sqrt{N}$. By setting \mathbf{b} as in Table 8, the linear system Equation (5.12) can be written in the form

$$(5.13) \quad K\lambda = \mathbf{b}$$

We solve Equation (5.13) using GMRES and report the initialization time, solution time in Table 31, memory and relative error in the solution in Table 32 for all the seven algorithms. We also plot the initialization time (Figure 20a), solution time (Figure 20b) and memory (Figure 20c) in Figure 20 to solve the Equation (5.13).

N	Initialization time (s)							Solution time (s)						
	$nHOD(b+t)$	$FMM(b)$	$s-nHOD$	$nHOD(t)$	$FMM(t)$	HOD	\mathcal{H}	$nHOD(b+t)$	$FMM(b)$	$s-nHOD$	$nHOD(t)$	$FMM(t)$	HOD	\mathcal{H}
8000	7.36295	6.54487	7.08227	7.88348	6.44558	4.27264	4.30182	0.16725	0.16764	0.16161	0.20728	0.17183	0.17014	0.17809
27000	39.3425	32.8879	35.6724	64.1132	32.9069	15.8539	15.2288	0.5375	0.55871	0.54972	0.60367	0.57584	0.65719	0.73221
64000	236.843	226.396	223.485	383.816	245.076	97.9317	106.53	3.03	3.55794	3.11424	3.04326	3.62864	3.66287	4.24849
125000	633.416	637.897	590.771	1230.98	747.517	203.94	216.759	6.34614	7.61801	6.71259	7.9912	7.81108	7.74681	7.91295
216000	1110.06	1156.01	1119.19	2760.7	1446.81	362.597	379.72	9.94425	12.0003	10.8462	11.3415	12.3137	15.035	16.7236
343000	2551.33	2814.72	2593.64	5484.89	3398.19	1006.16	1163.93	30.2831	39.9602	34.2393	37.802	39.7129	47.6998	75.7351
512000	4234.76	6102.69	4526.51	9759.81	5829.67	1521.21	1712.05	43.7953	69.6861	49.2419	64.4282	65.5984	75.2232	103.355
729000	7802.57	9123.71	-	-	-	2402.12	-	81.6482	145.19	-	-	-	160.174	-

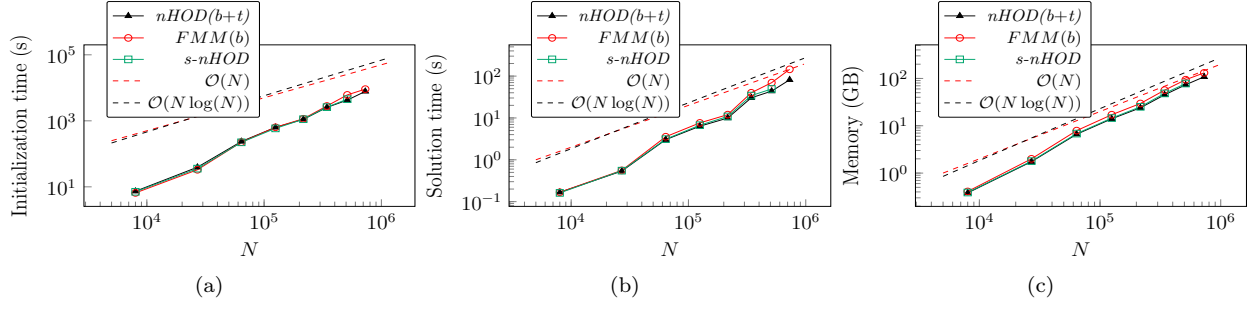
TABLE 31

Time comparison of the algorithms as mentioned in Table 7 for the Equation (5.13)

N	Memory (GB)							Relative error in solution (norm 2)							# it_e
	$nHOD(b+t)$	$FMM(b)$	$s\text{-}nHOD$	$nHOD(t)$	$FMM(t)$	HOD	\mathcal{H}	$nHOD(b+t)$	$FMM(b)$	$s\text{-}nHOD$	$nHOD(t)$	$FMM(t)$	HOD	\mathcal{H}	
8000	0.38098	0.40937	0.38867	0.40234	0.40937	0.40195	0.41849	1.18E-08	8.33E-09	9.54E-09	1.39E-08	8.33E-09	6.31E-09	4.13E-09	13
27000	1.74341	2.00058	1.78733	1.93888	2.00058	2.15085	2.43087	2.54E-08	1.29E-08	1.82E-08	3.45E-08	2.19E-08	9.15E-09	3.99E-09	15
64000	6.618	7.9008	6.83249	7.29892	7.84043	7.59349	8.39372	3.49E-08	2.61E-08	2.93E-08	3.80E-08	2.57E-08	9.73E-09	4.28E-09	17
125000	14.0367	17.1195	14.5407	17.5959	17.1272	16.5144	18.5576	4.99E-08	4.35E-08	4.09E-08	5.49E-08	3.38E-08	8.15E-09	5.50E-09	19
216000	23.9536	29.5657	25.1188	30.6623	29.5582	33.0032	38.0691	7.26E-08	5.45E-08	5.63E-08	7.03E-08	3.99E-08	2.22E-08	6.89E-09	21
343000	45.0993	56.6382	48.2667	53.4193	56.5565	68.6467	78.6682	8.92E-08	7.50E-08	7.20E-08	1.07E-07	4.04E-08	1.76E-08	5.30E-09	22
512000	73.4419	93.9927	78.1053	89.2306	92.9618	102.437	116.866	9.13E-08	5.55E-08	6.26E-08	1.09E-07	3.67E-08	1.55E-08	5.95E-09	24
729000	108.354	130.157	-	-	-	152.014	-	9.76E-08	4.36E-08	-	-	-	2.13E-08	-	25

TABLE 32

Memory and relative error in the solution of the algorithms as mentioned in Table 7 for the Equation (5.13)

FIG. 20. Various benchmarks of the algorithms $nHOD(b+t)$, $FMM(b)$ and $s-nHOD$ for the Equation (5.13)**Experiment 13.**

5.2.4. Fast matrix-vector product accelerated GMRES for integral equation in 3D. We consider the Fredholm integral equation of the second kind over $C = [-1, 1]^3 \subset \mathbb{R}^3$, which is given by

$$(5.14) \quad \sigma(\mathbf{x}) + \int_C F(\mathbf{x}, \mathbf{y}) \sigma(\mathbf{y}) d\mathbf{y} = f(\mathbf{x}) \quad \mathbf{x}, \mathbf{y} \in C$$

with $F(\mathbf{x}, \mathbf{y}) = \frac{1}{4\pi \|\mathbf{x} - \mathbf{y}\|_2}$ (Green's function for Laplace equation in 3D). We follow a piece-wise constant collocation method with collocation points on a uniform grid in $C = [-1, 1]^3$ with weights $1/N$ to discretize (5.14) and set the RHS \mathbf{f} as described in Table 8. Therefore, we obtain the following linear system

$$(5.15) \quad K\sigma = \mathbf{f}$$

We solve Equation (5.15) using GMRES and report the initialization time, solution time in Table 33 and memory, relative error in Table 34 for all the seven algorithms. We also plot the initialization time (Figure 21a), solution time (Figure 21b) and memory (Figure 21c) in Figure 21 to solve Equation (5.15).

N	Initialization time (s)							Solution time (s)						
	$nHOD(b+t)$	$FMM(b)$	$s-nHOD$	$nHOD(t)$	$FMM(t)$	HOD	\mathcal{H}	$nHOD(b+t)$	$FMM(b)$	$s-nHOD$	$nHOD(t)$	$FMM(t)$	HOD	\mathcal{H}
8000	3.19886	6.14962	10.9948	10.5071	3.97379	2.37187	3.05238	0.05665	0.09246	0.08627	0.08908	0.06636	0.07643	0.12441
27000	17.4942	28.2355	21.8527	55.6332	25.7309	7.96216	7.94475	0.18227	0.44748	0.22286	0.23588	0.21017	0.32257	0.33609
64000	102.586	170.215	110.467	252.483	175.28	70.0543	64.6349	0.88785	1.52783	1.36333	1.37966	1.08592	2.105	2.10945
125000	305.73	536.463	354.986	802.731	554.805	130.581	118.948	1.62647	2.80763	2.72584	2.45921	1.98636	4.18493	4.5363
216000	597.573	952.204	674.494	1759.74	1063.97	248.37	202.075	2.49224	4.02371	4.37228	3.80881	3.06654	8.4902	5.94086
512000	2161.56	3386.19	2593.56	7122.04	4055.28	1448.03	1005.03	9.74388	17.4997	17.2528	16.2378	12.4574	25.0419	28.5416
729000	3481.24	5700.3	4062.47	11609.7	6929.87	-	1496.1	11.1986	22.0292	20.4409	19.1133	16.4479	-	33.6336
1000000	5294	-	6076.27	-	10679.5	-	-	19.9203	-	34.95	-	29.8866	-	-

TABLE 33
Time comparison of the algorithms as mentioned in Table 7 for the Equation (5.15)

N	Memory (GB)							Relative error in solution (norm 2)							#iter
	$nHOD(b+t)$	$FMM(b)$	$s-nHOD$	$nHOD(t)$	$FMM(t)$	HOD	\mathcal{H}	$nHOD(b+t)$	$FMM(b)$	$s-nHOD$	$nHOD(t)$	$FMM(t)$	HOD	\mathcal{H}	
8000	0.29883	0.32811	0.30898	0.31349	0.32811	0.36322	0.38329	3.30E-10	1.62E-10	2.02E-10	3.42E-10	1.62E-10	1.88E-10	1.65E-10	5
27000	1.62294	1.9114	1.66382	1.74337	1.9114	2.02366	2.3258	2.87E-10	1.68E-10	1.74E-10	4.12E-10	1.68E-10	9.53E-11	2.68E-11	5
64000	4.98013	5.87951	5.21182	5.43848	5.86267	6.73525	7.50358	2.75E-10	1.62E-10	1.93E-10	5.52E-10	2.58E-10	8.47E-11	5.39E-11	5
125000	11.4558	13.9693	11.9985	12.8177	13.9527	14.8841	16.9177	3.67E-10	1.79E-10	1.59E-10	4.72E-10	1.68E-10	5.59E-11	2.48E-11	5
216000	21.0709	25.8782	22.1093	24.4137	25.8509	30.3117	35.3887	3.98E-10	1.87E-10	1.41E-10	6.72E-10	1.48E-10	4.99E-11	1.95E-11	5
512000	56.9231	70.0691	61.2259	68.1659	69.5588	91.5771	104.82	2.68E-10	1.22E-10	9.93E-11	4.73E-10	9.62E-11	5.42E-11	1.74E-11	5
729000	87.0228	109.157	93.8724	101.904	108.45	-	156.027	4.85E-10	1.35E-10	1.28E-10	4.52E-10	1.50E-10	-	9.10E-11	4
1000000	123.015	-	133.17	-	154.531	-	-	5.53E-10	-	1.11E-10	-	9.62E-11	-	-	5

TABLE 34
Memory and relative error in the solution of the algorithms as mentioned in Table 7 for the Equation (5.15)

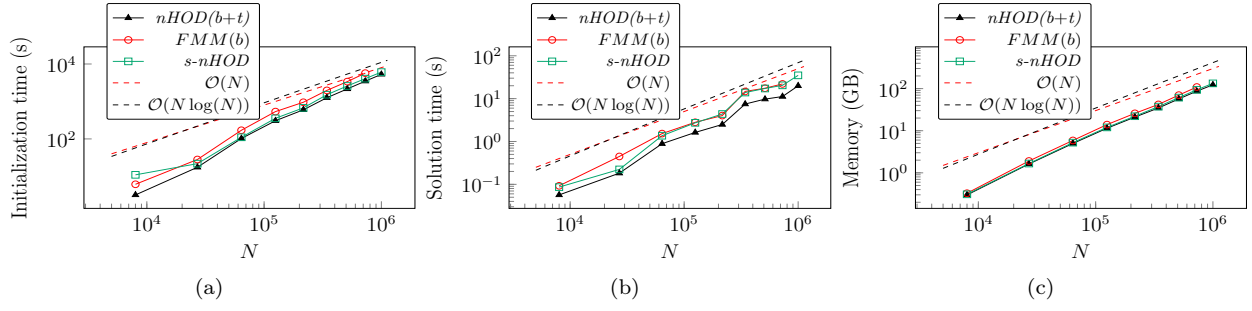


FIG. 21. Various benchmarks of the algorithms $nHOD(b+t)$, $FMM(b)$ and $s-nHOD$ for the Equation (5.15)

Remark 5.5. The proposed $nHOD(b+t)$ beats all the other algorithms in the context of the matrix-vector product time and memory in all the experiments for 3D problems too. It is to be noted that, among the nested algorithms, the initialization time of the $nHOD(b+t)$ is the fastest in 3D. Despite its initialization time roughly scaling as $O(N \log(N))$, the proposed $nHOD(b+t)$ still outperforms the algebraic FMM in 3D (initialization of $FMM(b)$ scales as $O(N)$) for $N \leq 2197000$ (the maximum value achievable in our system). The reason is as we go for the higher dimensional problems, the far-field interaction rank, as well as interaction list size, grow exponentially with the underlying dimension (but far-field rank scales as $O(1)$ with N), and the FMM structure has a larger interaction list and neighbors compared to the $nHODLRdD$ structure (Table 4). Hence, for the 3D problems, the initialization of $nHOD(b+t)$ is faster than that of the $FMM(b)$ for a reasonably large value of N . So, in the context of higher dimensional problems, $nHODLRdD$ might be more effective than the **algebraic** FMM.

Remark 5.6. The proposed $s-nHOD(b+t)$ and the $FMM(b)$ exhibit almost similar performance in terms of time in 3D. However, the $s-nHOD(b+t)$ outperforms the $FMM(b)$ slightly in terms of memory in 3D.

Remark 5.7. The initialization cost of the nested algorithms is higher than the non-nested algorithms in 3D because

1. The initialization of nested algorithms incorporates an inversion (Equation (3.3)) through the LU decomposition (LU decomposition is available as a byproduct of the ACA). This impacts the initialization time as the rank increases. On the other hand, the ACA used in the non-nested algorithm operates in the form UV^* , which involves no inversion; otherwise, if we consider only the NCA or ACA time to create the hierarchical structures, then NCA is faster than ACA.
2. Initialization time includes the assembly time of the M2L dense operators in the nested algorithms, whereas, in the non-nested algorithms, there are no such M2L operators. Our experiments in 3D show that the initialization time of the nested algorithms is high due to the impact of the increased size of the interaction list and the rank as dimensions grow, thereby affecting the overall initialization time.

Remark 5.8. We want to reiterate that there is room for further optimization, such as leveraging the symmetric property of the kernel matrix and incorporating translation invariant operators to reduce the initialization and memory cost. Nonetheless, the central theme here is maintaining uniformity in constructing all the 7 algebraic fast algorithms, including nested, semi-nested and non-nested variants. We have implemented all the algorithms in the same fashion using C++ and tested them within the same environment, allowing for meaningful comparisons.

We consolidate all the experiments and organize them in ascending order based on the initialization time, matrix-vector product time/solution time and storage in Table 35.

6. An efficient treatment for the dense M2L operators. The M2L (multipole to local) operation adds a big contribution to the computational cost in the $nHODLRdD$ algorithm (in fact, any \mathcal{H}^2 like algorithm). Performing the M2L operation multiple times for each cluster can lead to significant computational overhead. Computing the M2L operations for higher dimensional problems is a significant challenge as the number of dimensions increases, leading to a rapidly growing size of the interaction list and the rank. This section discusses an efficient treatment for the dense M2L operators because they possess a low-rank struc-

TABLE 35
Summary of the 13 experiments and the comparison among the 7 algorithms in Table 7

TABLE 35
Summary of the 13 experiments and the comparison among the 7 algorithms in Table 7

ture. We further re-compress the dense M2L operators by means of the ACA [5] in the form UV^* . Again, we rely on the ACA since it is cheaper than conventional techniques like truncated SVD or QR. Instead of storing the dense M2L operators, we store the U and V factors of the M2L operators and apply them to the vector, which results in faster computation and reduces the storage. To be precise, for a cluster, the storage and multiplication time cost of a M2L operator of size $p \times p$ scale as $\mathcal{O}(p^2)$ but after the re-compression using the ACA, this reduces to $\mathcal{O}(pp')$, where $U, V \in \mathbb{C}^{p \times p'}$. We compare the previous $nHODLRdD$ algorithm (M2L operators were not re-compressed, denoted as $nHOD(b+t)$, ref. Table 7) in the last experiment (Tables 33 and 34) over the $nHODLRdD$ algorithm with efficient treatment for the M2L operators (denoted as $effM2L$). In the $effM2L$ algorithm, we re-compress the M2L operators in such a way that the relative error in the solution remains almost the same as in Table 34; apart from the re-compression, all the other parameters remain same. The comparison results in Table 36 demonstrate that the $effM2L$ algorithm offers advantages over the previous $nHODLRdD$ algorithm ($d = 3$) in terms of computational time and memory usage. However, it is important to acknowledge that every algorithm has its trade-offs, and the $effM2L$ algorithm is no exception. While it outperforms the $nHOD(b+t)$ in time and space, there is a cost associated with the initialization phase due to the re-compression of the M2L operators.

N	Initialization time (s)		Solution time (s)		Memory (GB)			Relative error in solution	
	$nHOD(b+t)$	$effM2L$	$nHOD(b+t)$	$effM2L$	$nHOD(b+t)$	$effM2L$	$nHOD(b+t)/effM2L$	$nHOD(b+t)$	$effM2L$
27000	17.4942	33.8153	0.18227	0.17628	1.62294	1.48808	1.09	2.87E-10	3.90E-10
64000	102.586	198.311	0.88785	0.80791	4.98013	3.51092	1.418	2.75E-10	3.53E-10
125000	305.73	547.185	1.62647	1.06965	11.4558	7.75806	1.476	3.67E-10	3.19E-10
216000	597.573	993.195	2.49224	1.71544	21.0709	16.5598	1.272	3.98E-10	4.14E-10
512000	2161.56	3794.21	9.74388	6.1154	56.9231	36.9811	1.54	2.68E-10	2.47E-10
729000	3481.24	5766.56	11.1986	8.35332	87.0228	53.8028	1.617	4.85E-10	4.34E-10
1000000	5294.21	7090.25	19.9203	13.288	123.015	76.8404	1.601	5.53E-10	4.92E-10

TABLE 36

Comparison between the previous $nHODLR3D$ ($nHOD(b+t)$) and the $nHODLR3D$ with efficient M2L ($effM2L$) for the Equation (5.15) (Experiment 13)

7. Conclusion. This article presents two new fast matrix-vector product algorithms for N -body problems. The first is an efficient nested hierarchical matrix algorithm called $nHODLRdD$ ($nHOD(b+t)$), the nested version of the $HODLRdD$ algorithm. The second algorithm presents a semi-nested variant, known as $s-nHODLRdD$ ($s-nHOD$). Due to the use of the nested bases, the computational complexity is improved significantly. We evaluate the performance of our algorithms through extensive numerical experiments conducted in both 2D and 3D. We compare 2 proposed algorithms with 5 different fast matrix-vector product algorithms. Notably, all these algorithms are developed purely algebraically, making them kernel-independent. To our knowledge, this is the first work to study the performance analysis of different algebraic fast algorithms. Numerical results in 2D and 3D show that the $nHODLRdD$ is competitive with the algebraic FMM with respect to the memory and matrix-vector product time. So, this could be an alternative to the algebraic FMM. We also propose a cost-effective way to handle the dense M2L operators. Finally, we would like to release the implementation of the proposed $nHODLRdD$ and $s-nHODLRdD$ algorithms made available at <https://github.com/riteshkhan/nHODLRdD/>, the repository currently works for $d = 1, 2, 3$.

8. Acknowledgments. We acknowledge the use of the computing resources at HPCE, IIT Madras.

REFERENCES

- [1] S. AMBIKASARAN AND E. DARVE, *An $\mathcal{O}(n \log n)$ fast direct solver for partial hierarchically semi-separable matrices: With application to radial basis function interpolation*, Journal of Scientific Computing, 57 (2013), pp. 477–501.
- [2] S. AMBIKASARAN, J. Y. LI, P. K. KITANIDIS, AND E. DARVE, *Large-scale stochastic linear inversion using hierarchical matrices*, Computational Geosciences, 17 (2013), pp. 913–927.
- [3] P. AMESTOY, A. BUTTARI, J.-Y. L'EXCELLENT, AND T. MARY, *On the complexity of the block low-rank multifrontal factorization*, SIAM Journal on Scientific Computing, 39 (2017), pp. A1710–A1740.
- [4] J. BARNES AND P. HUT, *A hierarchical $\mathcal{O}(N \log N)$ force-calculation algorithm*, nature, 324 (1986), pp. 446–449.
- [5] M. BEBENDORF AND S. RJASNOW, *Adaptive low-rank approximation of collocation matrices*, Computing, 70 (2003), pp. 1–24.
- [6] M. BEBENDORF AND R. VENN, *Constructing nested bases approximations from the entries of non-local operators*, Numerische Mathematik, 121 (2012), pp. 609–635.

- [7] S. BÖRM, *Construction of data-sparse h^2 -matrices by hierarchical compression*, SIAM Journal on Scientific Computing, 31 (2009), pp. 1820–1839.
- [8] S. BÖRM, L. GRASEDYCK, AND W. HACKBUSCH, *Hierarchical matrices*, Lecture notes, 21 (2003), p. 2003.
- [9] S. BÖRM, L. GRASEDYCK, AND W. HACKBUSCH, *Introduction to hierarchical matrices with applications*, Engineering analysis with boundary elements, 27 (2003), pp. 405–422.
- [10] B. CARPENTIERI, I. S. DUFF, L. GIRAUD, AND M. MAGOLU MONGA MADE, *Sparse symmetric preconditioners for dense linear systems in electromagnetism*, Numerical linear algebra with applications, 11 (2004), pp. 753–771.
- [11] J. C. CARR, W. R. FRIGHT, AND R. K. BEATSON, *Surface interpolation with radial basis functions for medical imaging*, IEEE transactions on medical imaging, 16 (1997), pp. 96–107.
- [12] S. CHANDRASEKARAN, P. DEWILDE, M. GU, W. LYONS, AND T. PALS, *A fast solver for HSS representations via sparse matrices*, SIAM Journal on Matrix Analysis and Applications, 29 (2007), pp. 67–81.
- [13] S. CHANDRASEKARAN AND I. C. IPSEN, *On rank-revealing factorisations*, SIAM Journal on Matrix Analysis and Applications, 15 (1994), pp. 592–622.
- [14] W. FONG AND E. DARVE, *The black-box fast multipole method*, Journal of Computational Physics, 228 (2009), pp. 8712–8725.
- [15] A. GILLMAN, P. M. YOUNG, AND P.-G. MARTINSSON, *A direct solver with $O(N)$ complexity for integral equations on one-dimensional domains*, Frontiers of Mathematics in China, 7 (2012), pp. 217–247.
- [16] L. GRASEDYCK AND W. HACKBUSCH, *Construction and arithmetics of h -matrices*, Computing, 70 (2003), pp. 295–334.
- [17] A. GRAY AND A. MOORE, *N -body problems in statistical learning*, Advances in neural information processing systems, 13 (2000).
- [18] L. GREENGARD AND V. ROKHLIN, *A fast algorithm for particle simulations*, Journal of computational physics, 73 (1987), pp. 325–348.
- [19] L. GREENGARD AND V. ROKHLIN, *A new version of the fast multipole method for the laplace equation in three dimensions*, Acta numerica, 6 (1997), pp. 229–269.
- [20] V. GUJJULA AND S. AMBIKASARAN, *A new nested cross approximation*, arXiv preprint arXiv:2203.14832, (2022).
- [21] W. HACKBUSCH, *Hierarchical Matrices: Algorithms and Analysis*, vol. 49, 12 2015, <https://doi.org/10.1007/978-3-662-47324-5>.
- [22] W. HACKBUSCH, B. N. KHOROMSKIJ, AND R. KRIEMANN, *Hierarchical matrices based on a weak admissibility criterion*, Computing, 73 (2004), pp. 207–243.
- [23] K. L. HO AND L. YING, *Hierarchical interpolative factorization for elliptic operators: integral equations*, arXiv preprint arXiv:1307.2666, (2013).
- [24] V. A. KANDAPPAN, V. GUJJULA, AND S. AMBIKASARAN, *HODLR2D: A new class of hierarchical matrices*, arXiv preprint arXiv:2204.05536, (2022).
- [25] R. KHAN, V. KANDAPPAN, AND S. AMBIKASARAN, *HODLRdD: A new black-box fast algorithm for N -body problems in d -dimensions with guaranteed error bounds*, arXiv preprint arXiv:2209.05819, (2022).
- [26] E. LIBERTY, F. WOOLFE, P.-G. MARTINSSON, V. ROKHLIN, AND M. TYGERT, *Randomized algorithms for the low-rank approximation of matrices*, Proceedings of the National Academy of Sciences, 104 (2007), pp. 20167–20172.
- [27] L. LIN, J. LU, AND L. YING, *Fast construction of hierarchical matrix representation from matrix–vector multiplication*, Journal of Computational Physics, 230 (2011), pp. 4071–4087.
- [28] C.-T. PAN, *On the existence and computation of rank-revealing lu factorizations*, Linear Algebra and its Applications, 316 (2000), pp. 199–222.
- [29] C. E. RASMUSSEN, *Gaussian Processes in Machine Learning*, Springer Berlin Heidelberg, Berlin, Heidelberg, 2004, pp. 63–71, https://doi.org/10.1007/978-3-540-28650-9_4.
- [30] Y. SAAD AND M. H. SCHULTZ, *Gmres: A generalized minimal residual algorithm for solving nonsymmetric linear systems*, SIAM Journal on scientific and statistical computing, 7 (1986), pp. 856–869.
- [31] A. K. SAIBABA, S. AMBIKASARAN, J. Y. LI, P. K. KITANIDIS, AND E. F. DARVE, *Application of hierarchical matrices to linear inverse problems in geostatistics*, Oil & Gas Science and Technology–Revue d’IFP Energies nouvelles, 67 (2012), pp. 857–875.
- [32] J. XIA, *Multi-layer hierarchical structures*, CSIAM Transactions on Applied Mathematics, 2 (2021).
- [33] J. XIA, S. CHANDRASEKARAN, M. GU, AND X. S. LI, *Fast algorithms for hierarchically semiseparable matrices*, Numerical Linear Algebra with Applications, 17 (2010), pp. 953–976.
- [34] C. YANG, R. DURAISWAMI, N. A. GUMEROV, AND L. DAVIS, *Improved fast gauss transform and efficient kernel density estimation*, in Computer Vision, IEEE International Conference on, vol. 2, IEEE Computer Society, 2003, pp. 464–464.
- [35] L. YING, G. BIROS, AND D. ZORIN, *A kernel-independent adaptive fast multipole algorithm in two and three dimensions*, Journal of Computational Physics, 196 (2004), pp. 591–626.
- [36] R. YOKOTA, H. IBEID, AND D. KEYES, *Fast multipole method as a matrix-free hierarchical low-rank approximation*, in International Workshop on Eigenvalue Problems: Algorithms, Software and Applications in Petascale Computing, Springer, 2015, pp. 267–286.
- [37] Y. ZHAO, D. JIAO, AND J. MAO, *Fast nested cross approximation algorithm for solving large-scale electromagnetic problems*, IEEE Transactions on Microwave Theory and Techniques, 67 (2019), pp. 3271–3283.